Carbon nitride based photocatalysts for solar photocatalytic disinfection, can we go further?

Wenjun Wang[a, b], Chengyun Zhou[a, b], Yang Yang[a, b], Guangming Zeng[a, b, *], Chen Zhang[a, b, *], Yin Zhou[a, b], Jingnan Yang[a, b], Danlian Huang[a, b,], Han Wang[a, b], Weiping Xiong[a, b], Xiaopei Li[a, b], Yukui Fu[a, b], Ziwei Wang[a, b], Qingyun He[a, b], Meiying Jia[a, b], Hanzhuo Luo[a, b]

a College of Environmental Science and Engineering, Hunan University, Changsha, 410082, P.R. China

b Key Laboratory of Environmental Biology and Pollution Control, Ministry of Education, Hunan University, Changsha 410082, P.R. China

[*] Corresponding authors at: College of Environmental Science and Engineering, Hunan University, Changsha 410082, PR China.

E-mail addresses: zgming@hnu.edu.cn (G. Zeng), zhangchen@hnu.edu.cn (C. Zhang).

Contents

List of acronyms and abbreviations (Sort alphabetically)

Coenzyme A	CoA
Conduction band	CB
Cyclooctasulfur	α-S8
Density functional theory	DFT
Dissolved organic matter	DOM
Dissolved oxygen	DO
Electron paramagnetic resonance	EPR
Energy	ATP
Escherichia coli	*E. coli*
Expanded perlite	EP
G-C_3N_4@Co-TiO_2	CNCT
Glutathione	GSH
Gram-positive	G^+
Gram-negative	G^-
Graphene oxide	GO
Graphitic carbon nitride	g-C_3N_4
Hollow tubular g-C_3N_4	HTCN
Human adenovirus type 2	HAdV-2
Isopropanol	IPA
Natural organic matter	NOM
Nitroblue tetrazolium	NBT
One-dimensional	1D
Photodynamic antibacterial therapy	PDT
Porous g-C_3N_4 nanosheets	PCNS
Potassium ion	K^+
Quantum dots	QDs
Reactive oxygen species	ROS
Red phosphorous	r-P
Response surface methodology	RSM
Sodium oxalate	$Na_2C_2O_4$
Specific surface area	SSA
Staphylococcus aureus	*S. aureus*
Surface plasmon resonance	SPR
Terephthalic acid	TPA
Three-dimensional	3D
Titanium dioxide	TiO_2
Two-dimensional	2D
Valence band	VB
Visible-light-driven	VLD
World Health Organization	WHO
X-ray photoelectron spectroscopy	XPS
Zero-dimensional	0D
4-hydroxy-2,2,6,6-tetramethylpiperidinyloxy	TEMPOL

Abstract

Microbial contamination in wastewater systems is a global problem and has attracted more and more attention. Therefore, a high-performance and environmentally friendly inactivation method is in great demand. Graphitic carbon nitride (g-C_3N_4) exhibits lots of prominent properties such as appealing physicochemical stability, unique two-dimensional structure and tunable electronic structure. Unsatisfactorily, the pristine g-C_3N_4 also faces the shortcomings arising from the limited visible light response and few active sites. Hence, a comprehensive review ("can we go further?") about modified g-C_3N_4 photocatalysts for solar photocatalytic disinfection is necessary, which provides some inspiration for further optimization of the g-C_3N_4-based photocatalytic disinfection system. Meanwhile, the performance of g-C_3N_4-based photocatalysts for photocatalytic bacterial disinfection and the involved mechanisms are reviewed. In addition, the current prospects and possible challenges are pointed out. This review aims to summarize recent studies of g-C_3N_4-based photocatalysts in environmental disinfection and open a bright window to this booming research theme.

Keywords

Photocatalyst; Carbon nitride; Inactivation mechanisms; Bacteria

1. Introduction

Water pollution has become a global problem affecting human health [1-4]. Water-borne diseases are a public health problem that urgently needs to be addressed [5]. Pollutants in water mainly come from heavy metals in industrial wastewater, antibiotics in agricultural wastewater, bacteria in medical wastewater and organic matter in domestic wastewater, etc [6-8]. The World Health Organization (WHO) estimates that 80% of diseases in developing countries are caused by water contaminated by pathogenic microorganisms, including parasites, protozoa, fungi, bacteria, rickettsia, viruses, and prions [9, 10]. However, the applications of traditional disinfection methods (chlorination, ozonation, ultraviolet light irradiation and microbial degradation) are limited because of their huge energy consumption, expensive equipment and numerous disinfection by-products [11, 12]. Therefore, effective, low-cost and sustainable disinfection methods are urgently needed [13].

Fortunately, the advanced oxidation methods could oxidize and remove organic substances or bacterial by generating various reactive oxygen species (ROS) including •OH, H_2O_2 and $•O_2^-$ [14]. As one of the advanced oxidation methods, semiconductor photocatalytic technology ("green" method) could use ultraviolet or visible light to form a variety of ROS for energy generation, pathogen inactivation and contaminant degradation [8, 15-17]. Generally speaking, a photocatalytic reaction process mainly includes five steps [18-20] (Fig. 1): (i) semiconductor photocatalyst absorbs photons; (ii) excitation of semiconductor energy levels; (iii) separation process of electrons and holes in semiconductors; (iv) migration of electrons and holes in semiconductors; (v)

interface reaction. In 1985, Matsunaga *et al*. successfully used photocatalytic technology to kill a variety of bacteria including *Lactobacillus acidophilus*, *Saccharomyces cerevisiae* and *Escherichia coli* (*E. coli*) for the first time [21]. Since then, abundant photocatalytic systems have been well built for aqueous viruses inactivation, whereas the review of photocatalytic disinfection is still limited [22]. In different photocatalytic systems, it is important to choose the "suitable" semiconductor. In the early, titanium dioxide (TiO_2) has become the most commonly used nanomaterial for photocatalytic disinfection due to its non-toxicity, low price, high efficiency and stability [22]. Under the irradiation of ultraviolet light, TiO_2 mainly absorbs photons and promotes the separation of photo-generated electrons and holes, thereby generating ROS to inactivate microorganisms [23]. Nevertheless, there are still many challenges in using TiO_2-based semiconductor for photocatalytic disinfection due to its limited light absorption (corresponding to only ~4% sunlight utilization) [24]. Hence, a series of stable and robust visible-light-driven (VLD) photocatalysts to maximize the use of solar energy is needed.

Very recently, a metal-free organic polymeric nanomaterial (g-C_3N_4) has become the focus of VLD photocatalysis research, and it could be prepared from low-priced dicyanamide, cyanamide, thiourea, melamine and urea via thermal polymerization [25, 26]. Besides, it is well known that metal-free g-C_3N_4 possesses many unique properties (proper band gap, physicochemical stability, and good photoelectric characteristics), which might be caused by its heptazine ring structure or high condensation degree [27]. Lin *et al*. found that g-C_3N_4 nanosheets (a low toxicity

nanomaterials) could be regarded as drug carriers for cancer diagnosis and therapy, which is of great significance for photocatalytic disinfection [28]. Unsatisfactorily, the pristine g-C_3N_4 also faces the shortcomings arising from the limited visible light response, few active sites and swift recombination of photo-induced carriers [27]. So far, a lot of modification methods have been applied to conquer above limitations and enhance the capability of bulk g-C_3N_4, such as building co-catalyst systems and complicated heterojunctions, morphological control and self-modification (structural design) [23]. Besides, g-C_3N_4-based (modified) photocatalysts also show outstanding performance in other fields such as pollutant degradation, water splitting, nitrogen fixation, CO_2 reduction, and antibacterial treatment, etc [29-31]. For example, Wu *et al*. used g-C_3N_4-Zn^{2+}@GO hybrid nanosheets to kill bacteria and assist wound healing, which indicates that the use of g-C_3N_4-based materials for the photothermal effect and antibacterial treatment of sterilization has bright prospects [30].

In the past few years, some reviews about nanomaterials for photocatalytic inactivation were reported with the development of photocatalytic water disinfection, while the reviews summarizing g-C_3N_4-based photocatalysts for aqueous viruses' purification are still rare. In addition, the main influencing factors and mechanism of photocatalytic disinfection with g-C_3N_4-based photocatalysts are unclear in existing research. To fill above loopholes, a comprehensive review ("can we go further?") about g-C_3N_4-based photocatalysts for solar photocatalytic disinfection is necessary, which provides some inspiration for further optimization of the g-C_3N_4-based photocatalytic disinfection system. Firstly, the basic structure and properties of

g-C_3N_4 catalysts are summarized in this review, and how to design g-C_3N_4-based nanocomposites with better performance are also discussed. Meanwhile, numerous typical examples of various modified g-C_3N_4 photocatalysts applied in disinfection are mentioned, and the main mechanisms and vital influencing factors in this topic are also explored. Finally, the prospects and possible challenges are pointed out. This review is expected to inspire ongoing efforts to reasonably utilize the various nanostructures to construct more high-performance g-C_3N_4-based nanomaterials for microbial inactivation using endless sunlight energy, and open a bright window to this booming research theme.

2. Design considerations for carbon nitride-based photocatalysts

Systematic understanding of properties of g-C_3N_4 and the semiconductor photocatalytic reaction process are beneficial to construct g-C_3N_4-based nanomaterials with better photocatalytic capability. Notably, among the several allotropic forms of C_3N_4 (alpha phase, quasi cubic phase, cubic phase, beta phase and graphite phase), graphite C_3N_4 is deemed as the most stable phase at ambient conditions [32]. This is ascribed to its specific two-dimensional (2D) π-conjugated polymeric architecture which based on two basic units, s-triazine and tri-s-triazine rings. Moreover, Kroke and coworkers proved that tri-s-triazine-based structure is the most stable structure and energetically favored according to density functional theory (DFT) [33-35]. The 2D structure endows g-C_3N_4 with some promising and peculiar physical as well as electronic properties, supporting the application of g-C_3N_4 in environmental and

energy field. Weak van der Waals forces existed in layers provides the flake graphite characteristics, making the atoms in each layer arranged into a honeycomb structure with strong covalent bonds. The graphite like lamellar structure enables the transport of charge carriers and the mild energy gap (~2.7 eV) makes it workable at visible solar spectrum. The inherent electron-rich properties, hydrogen bond motifs and basic surface functionalities make it become a potential material in catalysis. Naturally, regarded as a conjugated polymer semiconductor, g-C_3N_4 has become a "hotspot" in environmental photocatalysis owing to its low cost, highly chemical stability and suitable electronic structure. Moreover, the specific properties (stability, optical and electronic properties, etc.) of g-C_3N_4 were provided in our previous research [36].

According to Fig. 1, the detailed process of the five steps of the photocatalytic reaction is as follows: First, the energy of the incident light must be greater than or equal to the band gap of the semiconductor, which will cause the electrons to be transferred to conduction band (CB) and then the holes to be generated on valence band (VB). Importantly, the semiconductor should possess adequate redox potential (appropriate location of CB and VB) for the desired photochemical reactions. Afterwards, the obtained electrons and holes will undergo a separation and transfer process in semiconductor. Accordingly, for better photocatalytic activity there must provide a driving force (electric field or magnetic field) to accelerate charge separation and boost the migration process. At last, the contaminants (bacterial, organic pollutions, and heavy metals, etc.) can react with photo-generated carriers in the surface of semiconductor, and the removal efficiency mainly counts on the

quantity of carriers and the redox ability of electron-hole pairs.

To form effective g-C_3N_4-based nanocomposites, some pivotal issues must be considered: (i) How to improve the light absorption efficiency of semiconductors? (ii) How to regulate the band structure of semiconductors? (iii) How to improve the efficiency of carrier's separation and migration? To conquer these barriers, corresponding measures should be taken: (i) Synthesis of special morphologies and nanostructures including different dimensions, core-shell structure and mesoporous structures of g-C_3N_4 to improve its specific surface area (SSA) and shorten the dispersal length of photo-generated carriers for better performance. (ii) Adjust the structure of g-C_3N_4 (metal doping, non-metal doping and defect engineering, etc.) to strengthen its VLD absorption capacity and redox capacity. (iii) Obtain the heterojunctions nanocomposites, construction the Schottky junction with built-in electrical potential and combination with co-catalysts (quantum dots or noble metals), helps to make better use of the advantages of the two semiconductors, thereby greatly improving catalytic activity of g-C_3N_4.

According to the analysis above, in order to improve the photocatalytic inactivation efficiency of g-C_3N_4-based photocatalysts, the main design considerations are focused on extending light absorption, enhancing SSA, improving active site density, and increasing the separation of photo-generated carriers. In the following section, g-C_3N_4 based photocatalysts are mentioned and classified into three different modification systems. Numerous typical examples and the latest progresses about these various modified g-C_3N_4 photocatalysts applied in photocatalytic disinfection

are summarized.

3. Recent advances in photocatalytic inactivation with carbon nitride-based photocatalysts

Pathogenic microbial contamination in aqueous solution has always been harmful to aquatic ecosystems and public health, which can cause millions of deaths each year [37]. Very recently, semiconductor photocatalytic inactivation has become the focus of antimicrobial research due to its unique properties like eco-friendliness and strong oxidation ability, which shows better performance than traditional bacterial disinfection approaches [38]. In recent years, amounts of work have been done on the application of g-C_3N_4-based nanomaterials in photocatalytic inactivation. Various kinds of g-C_3N_4-based nanomaterials display efficient photocatalytic capacity for removal bacterial, and the corresponding inactivation properties and the modification strategy are summarized in Table 1 and Table 2.

3.1 Morphology controlling

The structure of photocatalysts could be divided into several typical structures: mesoporous structure, zero-dimensional (0D), one-dimensional (1D), two-dimensional (2D), three-dimensional (3D), and core-shell structure, etc [39]. In general, vast studies have shown that photocatalysts with special nanostructures possess better activity than bulk materials, which may be due to size effects, multiple light scattering effect, larger SSA and enhanced reactant/product diffusion [22, 40]. In few decades, the exponential growth of the synthesis of various nanostructures and

their potential applications in photocatalytic bacterial disinfection has been witnessed. Among the above several nanostructures, the most popular is the 2D structure, mainly because of the following aspects: (i) the 2D nanostructure usually have more active sites due to its bigger SSA. (ii) the photo-generated carriers have a longer life, which is caused by the defects and considerably nonstoichiometry on the nanosheets surface [22]. (iii) most importantly, it is very simple to dominate the exposed active facets in the 2D nanostructure [41].

The pioneer work of Wang *et al*., for instance, reported that mesoporous g-C_3N_4 nanomaterials were prepared by hard templating method, exhibiting highly efficiency for *Escherichia coli* K-12 inactivation [42]. In this study, the SSA of mesoporous g-C_3N_4 (230 m^2 g^{-1}) was about a 20-fold increase compared to that of bulk g-C_3N_4 (12 m^2 g^{-1}) and the carriers could promote bacterial inactivation. The hard templating method or the soft templating method, nevertheless, involves expensive functional templates and complicated deletion processes, which are disadvantageous for practical applications. With above in mind, Zhu *et al*. used a template-free approach (no extra reagents) to prepare a porous g-C_3N_4 nanosheets (PCNS) with the SSA of 190.1 m^2 g^{-1} [41]. From Fig. 2a-d, it is observed that all *E. coli* (~100.0%) could be destroyed by PCNS under visible light irradiation (4 h), and the corresponding morphological structures of bacterial is shown in Fig. 2e-g. And the enhanced photocatalytic sterilization performance of PCNS might be ascribed to the enlarged band gap, the increased amounts of ROS, the bigger SSA, the well-developed porosity and decreased thickness [41]. Equally important, the high-quality g-C_3N_4 nanosheets with

a thickness of 15.4 nm were fabricated via a facile and clean bacteria-inspired bioexfoliation strategy under ambient temperature, reported by Kang *et al* (Fig. 2h) [43]. And the optimal g-C_3N_4 nanosheets presented an impressive photocatalytic disinfection effect (completely inactivated of *E. coli*), which indicated that the exfoliation of bulk g-C_3N_4 into g-C_3N_4 nanosheets exhibited effective charge transfer and excellent bacterial inactivation behavior.

Very recently, selectively introducing the electron-withdrawing groups onto the edge of g-C_3N_4 nanosheets (edge functionalization) could effectively boost the separation of carriers, assist production of H_2O_2 and induces an upward bending for enormous adsorption of oxygen molecules, thus improving disinfection efficiency [44-46]. Inspired by this strategy, Wang *et al*. synthesized an edge-functionalized g-C_3N_4 nanosheets (-COOH and C=O groups at the edge) as the photocatalysts to govern pathogen-rich wastewater, which exhibited an outstanding inactivation efficiency (nearly 100%) under 0.5 h visible-light irradiation with lower catalyst consumption [46]. The DFT calculations of edge-functionalized g-C_3N_4 nanosheets and schematic diagram of photocatalytic disinfection are depicted in Fig. 3a-c. DFT results showed that carbonyl and carboxyl groups changed the orbital state of adjacent carbon atoms, and proved that the functional groups on the edge can improve the efficiency of charge separation. From Fig. 3d-f, the edge functionalized g-C_3N_4 nanosheets were drop-casted on the internal surface of bags, which involved the contaminated water with 5.0 cm depth. In this study, the final sterilized wastewater could meet the China drinking water standards (GB5749-2006). In terms of

photocatalysis, the single-layer g-C_3N_4 nanosheet possesses better optical and electronic properties than multi-layer g-C_3N_4 nanosheets [47-49]. For example, Zhao *et al*. fabricated an atomic single layer g-C_3N_4 via thermal etching and ultrasonic exfoliation, and the activity of photocatalytic inactivation was investigated by destruction of *E. coli* (2×10^7 CFU/mL). Only ~5 log and ~3 log of *E. coli* can be inactivated on multi-layer g-C_3N_4 nanosheets and pristine g-C_3N_4, whereas all *E. coli* were destructed over the single-layer g-C_3N_4 nanosheet in a period of 240 min [47].

In addition to 2D or porous structures, g-C_3N_4 with different kinds nanostructure has been prepared for photocatalytic wastewater sterilization. Core shell structure is regarded as the novel structure for protecting the core ("guest" nanomaterial) from the surrounding environment, which maximized the contact area of two nanomaterials (Fig. 4a), enhanced the materialization stability and improved the catalytic performance [50-53]. Recently, Song *et al*. synthesized core shell structure of g-C_3N_4@Co-TiO_2 (CNCT) nanofibrous membranes via two-step process (electrospinning approach and thermal polymerization) (Fig. 4b) [54]. The as-obtained CNCT membranes presented a prominent antibacterial activity with a 6 log inactivation of *E. coil* within 1.5 h visible light irradiation, and corresponding disinfection efficiency, effect of dosage and SEM images of *E. coil* cells are described in Fig. 4c-g. The prominent photocatalytic performance benefits from the stable core-shell structures, enhanced visible-light response, maximum contact area and the effective charge transfer, etc. Similarly, for photocatalytic disinfection, 1D nanomaterials have attracted increasing attention due to their fast electron transport

efficiency (caused by 1D geometry), larger SSA (provide more active sites), enhanced light absorption (caused by high length-todiameter ratio) and fascinating physical properties, etc [55-57]. A unique structures of hollow tubular g-C_3N_4 (HTCN) were fabricated via a molecule self-assembly method by our group, and ~2.36-log destruction of *E. coli* cells by HTCN was obtained under visible light irradiation (40 min) [57]. The outstanding capability could be ascribed to the improved light utilization efficiency and decreased photo-generated e^-/h^+ recombination ratio. It is worth noting that studies on sterilization of 0D or 3D structure of g-C_3N_4 are scarce, and the researchers should pay more attention to this aspect. In summary, g-C_3N_4 with various nanostructures possesses more exposed active facets, bigger SSA, rapid carriers transfer efficiency, and shows great potential for photocatalytic water disinfection, which deserve further investigation. Moreover, the typical g-C_3N_4-based catalysts with various well defined nanostructured morphologies for photocatalytic sterilization are depicted in Table 1.

3.2 Structural design

The structural design is not the design of nanostructures, but the overall band gap configuration and surface modification of g-C_3N_4, which could hugely improve the photocatalytic activity of pure g-C_3N_4. Among them, the element doping (metal, nonmetal and co-doping) is the most promising strategy to adjust the band gap and electronic structure of g-C_3N_4, which satisfactorily enhance the carriers migration and broaden the light responsive range [58-62]. In recent few years, although lots of metallic impurities and non-metal element doped g-C_3N_4 have been studied in

photocatalytic applications, there have been scarce reports on photocatalytic virus disinfection [34]. There is an example about g-C_3N_4 nanosheets and red phosphorous (r-P) nanoparticle, and the obtained nanocomposites (CN/red phosphorous) presented better photo-disinfection performance than r-P and bulk g-C_3N_4 [63]. Recently, Zhang and coworkers used a simple low-temperature solvothermal-hydrothermal method to prepared the heterojunction photocatalysts of O-g-C_3N_4/HTCC (oxygen-doped g-C_3N_4 microspheres and hydrothermal carbonation carbon), which presented the excellent viricidal activity against human adenovirus type 2 (HAdV-2) within visible light irradiation [64]. The optimal heterojunction photocatalyst revealed the highest HAdV-2 viral inactivation efficiency (5-log), which was better than O-g-C_3N_4 (~ 1.5-log) and HTCC (~ 0.2-log). The above phenomenon was derived from the O-doping in the g-C_3N_4 lattice (induce intrinsic electronic and band structure modulation) and the uniform distribution of HTCC on the surface of O-g-C_3N_4 [58, 64, 65]. In this work, the corresponding band energy alignment and the Z-scheme mechanism diagram could be obtained in Fig. 5a. Till now, photocatalytic viral disinfection is still at its nascent stage for water treatment, but this pioneering work shed light on the developing more effective g-C_3N_4-based photocatalysts for wastewater treatment and highly resistant viral disinfection in practice. Notably, co-doping or tri-doping can combine the advantages of these single-doped atoms, leading to enhance the photocatalytic activity of g-C_3N_4 [66, 67]. For example, the nanocomposites of the silver particles (Ag) loaded on PSCN (phosphorus and sulfur co-doped g-C_3N_4) were constructed by calcination and biogenic-reduction procedures

with excellent sterilizing performance in water, researched by Xu *et al* [68]. As illustrated in Fig. 5b and Fig. 5c, all the nanocomposites of Ag/PSCN showed hugely enhanced inactivation activities as compared to bulk g-C_3N_4 and PSCN, but the excess deposited Ag (recombination centers) would reduce photocatalytic performance. The credible photocatalytic mechanism for destruction of *E. coli* with Ag/PSCN-4 was raised (Fig. 5d).

In addition, structure defect engineering, as a method of structural design, could regulate the light response characteristics and the surface band structure, which is helpful to improve the photocatalytic activity of pure g-C_3N_4 [69-71]. On the one hand, optimization of crystal structure of g-C_3N_4 is favorable for its electronic property and redox capacity of photo-generated charge carriers [72]. On the other hand, modification of surface property could efficiently controlling recombination rate of the carriers and increasing the adsorption of reactants on its surface, and thus accelerating the surface catalytic reactions [73, 74]. The study of Liu and colleagues, for instance, exhibited that the porous g-C_3N_4 nanosheets with nitrogen defects was successfully fabricated through thermal polymerization method (freeze-dried HCl-pretreated urea) [75]. As depicted in Fig. 6a-f, the existence of nitrogen defects was verified by DFT calculation, X-ray photoelectron spectroscopy (XPS), ^{13}C MAS NMR spectra and electron paramagnetic resonance (EPR) signals. Obviously, the optimized photocatalyst showed excellent pathogenic bacteria (*E. coli* and *Staphylococcus aureus* (*S. aureus*)) inactivation efficiency with the destruction of 4.80-log and 4.24-log, respectively. Further, in order to better observe the death of *E.*

coli, the confocal fluorescent images of live and dead bacteria were shown in Fig. 6g.

In the past few years, noble metal cocatalysts (Au, Ag, and Pd, etc.) have been considerably incorporated with g-C_3N_4 semiconductors, which could improve the photocatalytic performance through enlarging spectral response, separating charge carriers (electrons transfer) and the surface plasmon resonance (SPR) effect [76-81]. It is well-known that Ag is a promising bactericidal agent because of its beneficial roles (acceleration of carriers transfer and upshifting the VB of g-C_3N_4) [82, 83]. For example, Ma *et al*. introduced a photoreduction approach to obtain the hybrid Ag/g-C_3N_4 photocatalyst, which was used to destroy *E. coli* under light conditions. And it was confirmed through trapping experiments that e^-, h^+ and $\bullet O_2^-$ played a key role in the inactivation of *E. coli* cell [82]. Similarly, Xu *et al*. reported highly efficient antimicrobial performance against *S. aureus* by Ag-doped g-C_3N_4, and nearly all bacteria cells were destructed within 3 h visible light exposure [84]. Apart from Ag, by integrating of Au nanoparticles on the g-C_3N_4, a nanocomposite was prepared which exhibited considerably strengthened bactericidal activity in Gram-positive (G^+) and Gram-negative (G^-) bacteria removal [85]. Interestingly, the analysis of Fig. 7 exposed that Au/g-C_3N_4 could also efficiently resist wound infection and suppressing the creation of new biofilms in vitro. And others noble metal-based materials combinated with g-C_3N_4 were illustrated in section of heterojunctions. Furthermore, the latest g-C_3N_4-based photocatalysts with structural design for disinfection performances are also summarized in Table 1.

3.3 Heterojunctions and other g-C_3N_4-based system

Combining two different semiconductors into a heterojunction structure can not only effectively adjust the performance of a single semiconductor, but also produce many new features. Constructing g-C_3N_4-based hybrid heterojunctions to use solar energy is an attractive approach to improve the separation efficiency of charge carriers, thus promoting its photocatalytic performance [86-90]. Metal-free nanomaterials obtain much attention due to their multiple advantages (environmentally amicable and low cost), and it is extremely promising to build metal-free heterojunctions based on g-C_3N_4. In a pioneering research, Wang *et al*. synthesized a novel metal-free heterojunction photocatalyst (reduced graphene oxide and g-C_3N_4 cowrapped cyclooctasulfur (α-S8)), and the as-prepared samples exhibited good bacterial inactivation efficiency under visible light irradiation [91]. As shown in Fig. 8a-c, two different synthetic routes were applied to synthesized the two different heterostructures (RGOCNS8 and CNRGOS8), and their antibacterial activity were both much higher than g-C_3N_4 sheets under the aerobic or anaerobic conditions. Obviously, the two core−shell structure in the different nanocomposites played a critical role in controlling their photocatalytic disinfection performance and the different mechanisms were shown in Fig. 8d. This study proposed a new insight into the investigation and understanding the use of metal-free solar-driven photocatalytic wastewater inactivation. Graphene oxide (GO), regarded as another promising metal-free cocatalyst, could rapidly transfer carriers to its surrounding environment [92, 93]. The first report to record the antibacterial activity of GO/g-C_3N_4 was researched by Sun *et al*., and 97.9% of 10^7 CFU/mL of *E. coli* could be inactivated

within 120 min [94]. In another recent study, Ouyang *et al* prepared novel metal-free photocatalysts based on g-C_3N_4 and fullerene (C_{60}, C_{70}), which possessed unique electronic properties and applied for antimicrobial photodynamic disinfection [95]. Bulk g-C_3N_4 can only achieve bacterial inactivation efficiency of 68% under 240 min of visible light exposure, whereas as-obtained C_{60}/g-C_3N_4 and C_{70}/g-C_3N_4 nanocomposites destroyed 86% and 100% of *E. coli* O157:H7 cells, respectively. Above antimicrobials nanocomposites and others metal free photocatalysts could serve as a hopeful candidate for removing the bacteria in wastewater system.

Due to the tunable optical absorptivity, small size effect and good electrons transfer rates of quantum dots, thus the heterojunctions of quantum dots (QDs) as cocatalysts combined with semiconductor (mainly g-C_3N_4) have also been studied by numerous scientists [57, 96-99]. For example, Wang and co-workers used an ultrasonic method to prepared vanadate QDs ($BiVO_3$ and $AgVO_3$) embedded g-C_3N_4, and the inactivation efficiency of $BiVO_3$ QDs/g-C_3N_4 and $AgVO_3$ QDs/g-C_3N_4 could reach to 84% and 96.4% towards G^- *Salmonella* H9812 under 10 min of light illumination, respectively (Fig. 9a) [96]. From the results of Fig. 9b-d, the bactericidal efficiency of $AgVO_3$ QDs/g-C_3N_4 nanocomposites enhanced with increasing catalyst dose. They also found the neglected antimicrobial activity of $AgVO_3$ QDs, $AgVO_3$ QDs/g-C_3N_4 and $BiVO_3$ QDs/g-C_3N_4 in dark condition, which indicates the non-toxic of afore-mentioned nanomaterials (Fig. 9g-h). Furthermore, the temperature of the photocatalytic reaction system was measured via a thermal imager, which is a vital condition for bacterial survival under light illumination. From Fig. 9e-f, only 2.9 ℃

increased (from 27.2 ℃ at 5 min irradiation to 30.1 ℃ at 30 min irradiation) during the experiment, demonstrating the temperature stability of this system. For the first time, Li *et al*. synthesized VLD g-C_3N_4 QDs/ TiO_2 nanotube array membrane, which displayed improved anti-fouling activity in filtering wastewater with *E. coli* because of the synergistic effect of photocatalysis and membrane filtration [100]. Another example was the hollow tubular g-C_3N_4 which could capture the carbon QDs for *E. coli* inactivation, reported by our team [57]. The schematic illustration of the preparation for hollow tubular g-C_3N_4 capture the carbon QDs is described in Fig. 9i, and the optimal sample exhibited superior performance with 99.99% destruction of *E. coli* in 40 min of visible light irradiation. The above results provide new clues for designing 0D semiconductor/g-C_3N_4 heterojunction photocatalysts for photocatalytic disinfection.

Until now, many metal oxides and composite oxides have been attached with g-C_3N_4 for better bacteria sterilization performance under visible light illumination [101-103]. Among the diverse oxides semiconductors, TiO_2 has been regarded as the most suitable candidate to be integrated with g-C_3N_4. For the first time, Li *et al*. smoothly prepared g-C_3N_4/TiO_2 heterojunction and its bandgap was narrower than pure g-C_3N_4 and TiO_2, which presented outstanding photocatalytic activity for *E. coli* destruction [102]. From the results of potassium ion (K^+) leakage (concentration of K^+ increases with the photocatalytic reaction time increases), the bacteria cell membrane permeability and intact cell structure was destructed by ROS. Inspired by the above results, Xu *et al*. used novel heterojunction (aligned TiO_2 nanotube arrays loaded on

the g-C_3N_4 nanofilms) to destruction of *E. coli*, and the binary nanocomposites exhibited a significant bactericidal effect [104]. Moreover, the photocatalyst of g-C_3N_4/ZnO also possess great photocatalytic antimicrobial (towards *S. aureus* and *E. coli*) efficiency, proved by Sundaram *et al*. [105]. Very recently, a Z-scheme heterostructure of g-C_3N_4/MnO_2 on the surface of metallic Ti implants was constructed (Fig. 10a) and displayed superior antibacterial efficiency of 99.26% and 99.96% against *E. coli* and *S. aureus* severally (Fig. 10b-c), in which MnO_2 enhanced the photocatalyst activity of g-C_3N_4 to obtain more ROS and consume glutathione (GSH) to enhance inactivation efficiency [103]. The destruction of bacterial membrane and the leakage of protein were proved that more ROS could be generated in the g-C_3N_4/MnO_2 heterostructure (Fig. 10d-f). Furthermore, GSH in bacteria will be oxidized by MnO_2 in the coating, enhancing the efficiency of photodynamic antibacterial therapy (PDT), the corresponding loss diagram of GSH and mechanism graph was shown in Fig. 10g-i. Similarly, the composite oxides $MgTi_2O_5$ was chosen to attach g-C_3N_4 nanosheets via in situ growth strategy, and the obtained Z-scheme heterojunction $MgTi_2O_5$/g-C_3N_4 exhibited excellent *E. coli* inactivation effectiveness (7-log inhibition within 3 h) [106]. In the photocatalytic inactivation system, $\bullet O_2^-$ and H_2O_2 played the dominant role and •OH and h^+ played the moderate role, which confirmed by species trapping experiments. The proposed mechanism of $MgTi_2O_5$/g-C_3N_4 system is also depicted in Fig. 10j. Meanwhile, Ag-based composite oxides also have a wide range of applications in photocatalytic sterilization [107-110]. For instance, Li *et al*. synthesized a Ag_2WO_4/g-C_3N_4 nanocomposite via the

deposition-precipitation method, and the sample of Ag_2WO_4(5%)/g-C_3N_4 could remove 100% live bacteria within 1.5 h visible light irradiation [107]. Expanded perlite (EP), as a natural mineral (mainly contains Al_2O_3 and SiO_2), has several merits such as low cost (earth-abundant element), large particle sizes (higher SSA) and high photocorrosion resistance, etc [111]. Due to the above advantages, Li's group firstly developed water-surface-floating (g-C_3N_4/EP) photocatalytic nanocomposites for destruction of microorganism, and systematically studied water quality parameters for their potential application [111]. As previously mentioned, these researches demonstrate a proof-of-concept for developing antimicrobials with metal oxides and other complicated oxides for wastewater disinfection and microbial control.

Bismuth-based photocatalysts (such as bismuth oxyhalide (BiOX, X = Cl, Br, or I), bismuth oxides, $BiVO_4$ and Bi_2MoO_6, etc.) possess narrow bandgap, unique crystalline structures and excellent capacity of visible light absorption. Therefore, they gained extensive attention in photocatalytic field [112-117]. Recently, the Bi_2MoO_6/g-C_3N_4 heterojunctions were prepared based on g-C_3N_4 nanosheets via in situ solvothermal method, researched by Yin's team, which antibacterial capacity was better than g-C_3N_4 sheets and pure Bi_2MoO_6 [118]. The photocatalytic disinfection efficiency of various photocatalysts was revealed in Fig. 11a-b, and the representative antibacterial process was also shown in Fig. 11c. From Fig. 11a-b, the disinfection activity of Bi_2MoO_6/g-C_3N_4 heterojunctions were all higher than individual Bi_2MoO_6 and bulk CN, and the sterilization performance of g-C_3N_4 sheets was obviously promoted but still had room for further enhancement. Furthermore, the authors also

illustrated that the sterilization curve was divided into three parts: initial delay implied, log-linear disinfection region and an obvious deceleration process [118]. BiOBr has a tetragonal PbFCl-type layered crystal structure composed of $[Bi_2O_2]^{2+}$ plate and double plate of halogen atoms, which can improve the effective separation and movement of carriers [76, 119]. In Ni's research, the nanocomposite of BiOBr/g-C_3N_4 was prepared through a depositing method, and the obtained heterojunction exhibited outstanding photocatalytic disinfection activity towards to inactivated *E. coli* [120]. In addition, Wong *et al*. fabricated a monoclinic-Bi_2O_4/g-C_3N_4 heterostructure (Fig. 11d) that followed the Z-scheme photocatalytic mechanism (Fig. 11e) to removal *E. coli* within visible light [121]. Based on the Z-scheme mechanism, the e^- on the CB of g-C_3N_4 could efficiently obtain H_2O_2 and •OH via O_2 reduction due to its higher reducing power. From the sterilization curve (Fig. 11f), the monoclinic-Bi_2O_4/g-C_3N_4 heterostructure could completely removal *E. coli* (6-log) within 1.5 h, whereas 4-log and 1.5-log reduction of *E. coli* was received under 2 h light irradiation for monoclinic-Bi_2O_4 and g-C_3N_4, respectively.

For better develop the physicochemical properties of g-C_3N_4, the ternary or more complex design of g-C_3N_4 (consist of three or more components) antimicrobials have been proposed. Notably, this novel design of g-C_3N_4 antibacterial materials could make full of synergistic effects of multicomponent to uncommonly improve the separation efficiency of the carriers. It should be noted that the most common ternary structure of g-C_3N_4-based composite is g-C_3N_4/noble metals/semiconductor [122-127]. Very recently, Zeng *et al*. constructed a Z-scheme g-C_3N_4/Ag/$BiVO_4$ nanocomposite

for removal *E. coli* cells in simulated wastewater and sewage [126]. In this ternary system, noble metals (Ag) could decrease the recombination of carriers, boosted the interfacial electron transfer and promoted the generation of ROS. Therefore, the photocatalytic disinfection of ternary composite (g-C_3N_4/Ag/$BiVO_4$ 6.5-log) is obviously better than binary composite (g-C_3N_4/$BiVO_4$ 0.5-log) under 1 h of visible light irradiation. However, the existence of natural organic matter (NOM) in sewage is the main reason for reducing the photocatalytic bactericidal activity of g-C_3N_4/Ag/$BiVO_4$ nanocomposite. Another classic ternary structure of g-C_3N_4-based composite is g-C_3N_4/semiconductor/semiconductor [128-132]. For example, about 100% of *E. coli* cells could be inactivated by BiOBr/BiOI/g-C_3N_4 nanocomposite, whereas BiOBr, BiOI and g-C_3N_4 photocatalysts killed 29.4%, 34.2%, and 83.7% of *E. coli* under the visible light exposure, respectively [132]. The disinfection performance of the g-C_3N_4/TiO_2/kaolinite composite is significantly better than that of the g-C_3N_4 and TiO_2, which is a similar result obtained by Li *et al* [133]. Through all the analysis above, we have to admit that one modification method cannot significantly improve the performance of bulk g-C_3N_4, which encouraged us must adopt a combination of multiple modification strategies to enhance their photocatalytic activity. At last, amounts of recent g-C_3N_4-based heterojunctions materials for photocatalytic inactiviation are summarized in Table 2.

4. Influencing factors

In view of the lack of uniform specifications for the design of g-C_3N_4-based

photocatalysts, we summarize the factors that may affect its antibacterial activity as follows (Fig. 12a): (i) bacterial (types and concentrations); (ii) photocatalysts (nanostructure and sample loading); (iii) light conditions (light sources, light intensity and light wavelength); (iv) water qualities (dissolved oxygen (DO), dissolved organic matter (DOM), temperature, pH, inorganic ions, etc.). Analysis of these influencing factors will help us to further improve the efficiency of carbon nitride photocatalytic disinfection.

For the aspect of bacterial (i), because of the different size, shape, composition and structure, various types of viruses present different resistances to inactivation in photocatalysis [134]. In general, the sensitivity of bacterial species to photocatalysis is sorted from strong to weak as follows: G^- bacteria > G^+ bacteria > Yeast > Mold (filamentous fungi) [134, 135]. This sensitivity difference is mainly determined by the cell wall structure (complexity and thickness) and the resistance of cell wall components to oxidative damage [136-138]. Specifically, the cell wall thickness of G^+ bacteria is 2-8 times that of G^- bacteria. Therefore, G^+ bacteria have more peptidoglycan (one of the cell wall structures), which is the main substance against ROS. The initial concentration of bacteria also has a direct impact on the experimental results [139]. When the initial concentration of bacteria reaches 1×10^3 CFU/mL, the initial concentration has almost no effect on the sterilization rate. But when the initial concentration exceeds 1×10^8 CFU/mL, the photocatalytic activity may be reduced because of screen effect (reduces the light intensity that can be received in the cytoplasm) [140].

For the aspect of photocatalysts (ii), the nanostructure of carbon nitride photocatalysts has a direct impact on the efficiency of photocatalytic disinfection. Carbon nitrides with various nanostructures have different properties and therefore exhibit different photocatalytic activities. Specific modification measures have been mentioned in "Morphology controlling". Moreover, consistent with other photocatalytic applications, there also exists an optimal loading of g-C_3N_4-based photocatalysts for wastewater bacteria disinfection [141, 142]. Increasing the loading of g-C_3N_4 can provide more active site and improve the inactivation efficiency. However, exceeding the optimal loading of g-C_3N_4 will reduce the disinfection efficiency, which is caused by the reduced light penetration in water.

For the aspect of light conditions (iii), the pristine g-C_3N_4 has limited visible light response. Therefore, many modification strategies were applied to enhance the utilization of visible light of bulk g-C_3N_4. Fortunately, some g-C_3N_4-based photocatalysts have strong solar energy utilization (near-infrared light absorb), and the light source effect changes with the optical properties of photocatalysts [143, 144]. In the case of sunlight intensity, the maximum intensity of natural sunlight reaching the Earth's surface is about 1000 W/m^2, but the true intensity varies with various factors (season, weather, geographical location, etc.) [136, 145]. For example, Pulgarin *et al*. found that the inactivation efficiency of semiconductor photocatalysts increased with the increased light intensity [145]. Nonetheless, higher light intensity does not mean better inactivation efficiency, because higher light intensity could cause the waste of energy and lead to increased recombination of photo-generated carriers [142]. The

relationship between light wavelength and sterilization efficiency is not well understood, but few studies have shown that long-wavelength light has a better sterilization effect [146].

For the aspect of water qualities (iv), some important water factors like temperature, DO, pH, DOM, and inorganic ions on photocatalytic sterilization should be considered. In the Li' group, it has been reported that the effect of common ambient temperature (1.48 – 43.52 °C) on virus inactivation efficiency via g-C_3N_4 system is negligible [10]. Furthermore, Li *et al*. used response surface methodology (RSM) to optimize the different operating parameters (reaction temperature, light intensity and photocatalyst loading) for destruction of bacteriophage MS2 under visible light irradiation [10]. From Fig. 12b, under the optimized conditions of reaction temperature (24.05 ℃), metal loading (135.4 mg/L), and light intensity (199.8 mW/cm^2), the viruses can be killed up to 6.58 log PFU/mL. According to photocatalytic reaction process, increasing the amount of DO in the water is conducive to the production of ROS, thereby improving the photocatalytic disinfection activity [111]. Nevertheless, the improvement for bacterial inactivation with floating system was limited, because the air-water interfaces was easily access sufficient oxygen gas. As for pH, lowering the pH promotes antibacterial effects because of the synthesis of acid shock proteins in bacteria, but this trend does not apply to virus inactivation [147-149]. For example, Zhang *et al*. found that the g-C_3N_4/EP-520 photocatalysts were more beneficial for virus (MS2) inactivation at lower pH values, which may be due to the decrease in electrostatic repulsion between

photocatalysts and viruses [111].

As for DOM, the presence of organic impurities reduces photocatalytic sterilization rate via inhibiting the generation of ROS [150]. On the one hand, smaller-molecular-weight DOM could consume ROS in photocatalytic reactions, thus reducing ROS that react with bacterial. On the other hand, larger-molecular-weight DOM could form a protective layer on the surface of microorganisms to protect bacterial from photocatalytic inactivation [151]. Partial inorganic ions have a significant effect on the performance of photocatalytic disinfection, especially Fe^{2+}, Co^{2+}, and Cu^{2+} can greatly improve the photocatalytic efficiency via Fenton reaction and/or Fenton-like reaction [152]. In contrast, other inorganic ions (PO_4^{3-}, Ca^{2+}, SO_4^{2-}, and CO_3^{2-}) could inhibit bacterial inactivation via competitive adsorption activity sites on the surface of g-C_3N_4 and capture free radicals [59, 153], whereas some ions such as Na^+, Cl^-, and Br^-, etc. have negligible effects on photocatalytic disinfection [154]. To sum up, the above results unveil that the photocatalytic disinfection efficiency can be affected by many factors, and researchers should explore the optimal bactericidal conditions through extensive research.

5. Photocatalytic inactivation mechanisms

As mentioned in section 2, the photocatalytic reaction process involves five steps (Fig. 1), and the photocatalytic inactivation mechanism of g-C_3N_4 is explained by the generation of photo-induced charge carriers under visible light irradiation. Overall, electrons migration and generation of ROS species on g-C_3N_4 surface are illustrated

via following formulas (1–6) [34, 155-157].

$$g\text{-}C_3N_4 + h\nu \longrightarrow g\text{-}C_3N_4\ (e^- + h^+) \quad (1)$$

$$g\text{-}C_3N_4\ (h^+) + H_2O \longrightarrow g\text{-}C_3N_4 + \bullet OH + H^+ \quad (+2.38\ \text{eV vs NHE}) \quad (2)$$

$$g\text{-}C_3N_4\ (h^+) + OH^- \longrightarrow g\text{-}C_3N_4 + \bullet OH \quad (+1.99\ \text{eV vs NHE}) \quad (3)$$

$$g\text{-}C_3N_4\ (e^-) + O_2 \longrightarrow g\text{-}C_3N_4 + \bullet O_2^- \quad (-0.33\ \text{eV vs NHE}) \quad (4)$$

$$\bullet O_2^- + \bullet HO_2 \longrightarrow \bullet OH + O_2 + H_2O_2 \quad (-1.18\ \text{eV vs NHE}) \quad (5)$$

$$g\text{-}C_3N_4\ (e^-) + H_2O_2 \longrightarrow g\text{-}C_3N_4 + OH^- + \bullet OH \quad (+0.73\ \text{eV vs NHE}) \quad (6)$$

Generally speaking, the key ROS species in the photocatalytic disinfection process are H_2O_2, •OH and $\bullet O_2^-$, which can effectively react with cellular compounds, leak the cell wall membrane of microorganisms, and finally lead to cell death [34, 158-160]. However, the ROS that play a major role in different systems are uncertain. Hence, for the purpose of understanding the photocatalytic bactericidal mechanism, we should identify the major ROS formation from g-C_3N_4-based photocatalysts systems and their roles in bacterial destruction, as well as to know how the ROS lead to the destruction of bacterial cells.

Facile ROS trapping experiments could identify the major ROS in different photocatalytic bactericidal systems [22, 161-163]. In general, several scavengers such as isopropanol (IPA), sodium oxalate ($Na_2C_2O_4$), Fe(II)-EDTA, Cr^{6+} and 4-hydroxy-2,2,6,6-tetramethylpiperidinyloxy (TEMPOL) were added in photocatalytic bacterial inactivation or photocatalytic degradation pollutions and act as quenchers of •OH, h^+, H_2O_2, e^- and $\bullet O_2^-$, respectively [164-166]. The trapping experiments were applied to determine the major ROS with or without the partition

system, and the role of specific ROS in bacterial inactivation can be identified. Furthermore, the concentration of reactive species like •OH, $•O_2^-$ and H_2O_2 could be quantitatively determined via terephthalic acid (TPA) probe means, nitroblue tetrazolium (NBT) transformation method and iodometry [126, 164]. For example, in a $BiVO_4$/Ag/g-C_3N_4 photocatalytic system, Zeng *et al*. concluded that h^+ and $•O_2^-$ followed by H_2O_2 played important roles in photocatalytic bacterial inactivation via trapping experiments (Fig. 13a). The authors also demonstrated that the produced amount of reactive species $•O_2^-$, •OH and H_2O_2 by ternary $BiVO_4$/Ag/g-C_3N_4 was higher than that of the binary nanocomposite (Fig. 13b-d) [126]. Notably, for maximum scavenging effect during the photocatalytic bactericidal process, the applied concentrations of the scavengers should be controlled and optimized because of their potential toxicity to bacterial cells.

To further study the mechanism of g-C_3N_4-based nanocomposites photocatalytic bacterial inactivation, the cell membrane integrity variation of bacterial, release of intracellular substance (such as K^+, nucleic acids and antioxidant enzymes, etc.) and energy (ATP) synthesis are explored [106, 155, 156]. First of all, the bacterial cell inactivation is originally proposed to consume coenzyme A (CoA) through dimerization and subsequent inhibition of respiration (photocatalytic reduction process) [21, 22, 167]. Superoxide dismutase (SOD) and catalase (CAT), act as indicators for the oxidative stress encountered by the cells, are further investigated (photocatalytic oxidation process). Because SOD could catalyze the dismutation of $•O_2^-$ to H_2O_2 or O_2, and CAT could catalyze the dismutation of H_2O_2 to water and

oxygen to protect the bacteria [168-170]. For example, the SOD and the peroxidation intermediate MDA was measured to evaluate the bacterial membrane oxidation degree, studied by Jiang and co-workers (Fig. 13e) [106]. During the first 1.5 h, the MDA concentration increased, indicating that the lipid content was gradually oxidized, causing damage to the cell membrane. However, the concentration of SOD suggested the existence of antioxidant system and then damaged with the destructed of bacterial cells. Furthermore, most of the studies focus on microscopic analysis (SEM or TEM) to clearly observe the changes of bacterial morphology and confirm the destruction of bacterial cells during photocatalytic sterilization (like aforementioned Fig. 10d).

Overall, key ROS species attack cells and cause damage to membranes and cell walls. As we all know, K^+ is an important inorganic element in bacterial cells and is used for the regulation of proteins and polysomes [156, 171]. The concentration of K^+ could regarded as an index to evaluate cell membrane permeability, and in our previous work, the leakage of K^+ was detected to gradually increase with the visible light irradiation time increased, which indicates the breakage of cell membranes (Fig. 13f) [57]. Besides, other substances such as DNA, RNA, enzymes, carotenoid, glutathione, and peroxidase, may also involve defending against oxidative stress processes. From Fig. 13g-i, the results of the fluorescent intensity of genomic DNA and the leakage of DNA and RNA contents display that amounts of nucleic acids were liberated to the extracellular within the photocatalytic disinfection [106]. In addition, energy (ATP) synthesis is significant for cell repair and growth, hence, the handicap of ATP production would harm the bacterial metabolism. In the study of Xia *et al*., the

level of ATP decreased from 123.8 RLU/10^3 to 0, which demonstrated that the structure and metabolism of bacterial cells were damaged after the exposure to visible light irradiated g-C_3N_4/m-Bi_2O_4 within 60 min [121].

Taking together, above results indicate that the ROS attack the cell and ultimately destroy the bacterial cell. As displayed in Fig. 13j, the bacterial (like G^- *E. coli*) inactivation processes explored by g-C_3N_4-based nanocomposites within visible light irradiation, which mainly caused by chemical oxidation (ROS) mechanism? There are two other mechanisms (physical damage and the toxicity of metal ions based on metal-containing semiconductor) that have been studied by many researches [142]. Nonetheless, physical damage in virus inactivation usually involves GO-based photocatalysts, where GO has many sharp edges to destroy and inactivate the viral protein coat [172, 173]. As mentioned in section 4, the metal-based materials combined with g-C_3N_4 could improve the photocatalytic disinfection performance, because of the synergistic effect of photocatalysis and metal ion toxicity [174, 175]. Similarly, understanding photocatalytic inactivation mechanism of g-C_3N_4 will help us to further improve the efficiency of carbon nitride photocatalytic disinfection.

6. Summary and prospects

In summary, the solar-powered photocatalysis certainly represents one of the most promising technologies for wastewater disinfection. Unsatisfactorily, the pristine g-C_3N_4 shows poor performance in photocatalytic disinfection due to its limited visible light response, few active sites and swift recombination of light-induced

carriers. In present review, three different modification systems (morphology controlling, structural design and heterojunctions, etc.) based on g-C_3N_4 nanomaterials were summarized in detail. And it has been observed that the modified g-C_3N_4 nanocomposites present superior photocatalytic disinfection efficiency due to their larger SSA, better light utilization efficiency and slowly recombination of carriers, etc. Meanwhile, the performance of photocatalytic viral disinfection for g-C_3N_4-based photocatalysts and the key mechanisms of this subject are summarized. It is anticipated that the g-C_3N_4-based photocatalysts will become a research hotspot and this study aims to open a bright window to this booming research theme.

Although theoretical design is proposed and some considerable progress has been achieved, researches in this field and their development in practical applications are still in infancy and remain many challenges. First, in a photocatalytic system, the interface properties of the photocatalysts determine their final efficiency. So, it is critical to understand the carriers' generation, separation and migration across these nanoscale interfaces. As we all known, it is easy to understand the separation and migration of carriers in a simple g-C_3N_4 systems, but it is becoming increasingly difficult to understand and control the charge transport in multi-component complex structures based on modified g-C_3N_4, particularly on the nanometer scale. Naturally, the mechanisms of photocatalytic disinfection by the g-C_3N_4-based complex nanocomposites systems are partly uncertain. The detailed mechanism research of the carriers transfer process in multi-component complex system (three or more

components) is insufficient and will be necessary to further develop the photocatalytic disinfection field.

Secondly, most of the g-C_3N_4-based photocatalytic inactivation application have been proposed and studied in under laboratory conditions. For achieve future large-scale applications, amounts important issues such as catalyst immobilization, recycling methods, optimization of disinfection parameters and photocatalytic reactor design need to be addressed. Moreover, based on practical applications, the stability of g-C_3N_4-based nanomaterials also needs to be considered. DFT calculation is an essential tool in scientific research, which guide the modification of g-C_3N_4 and helps to predict photocatalytic reaction pathways. Hence, synthesizing innovative, efficient and stable g-C_3N_4-based nanocomposites via DFT technology is necessary. In addition to microorganisms in wastewater, the removal of the bacteria in the indoor/outdoor air and protozoa in the aqueous solution should also be stressed

Thirdly, as is also well known, microbes in nature are not all harmful, and some of them are good for humans. However, according to the mechanism of photocatalytic disinfection, various microorganisms (whether harmful or not) will be removed by ROS without prejudice and there is no oxidation selectivity. To this end, considerable effort is required to design molecularly imprinted photocatalysts based on specific cell surfaces to efficiently selectively inactivate specific microorganisms.

Finally, various advanced photocatalytic materials have appeared in few decades with the rapid development of nanotechnology. Interesting properties might be probed by integrating the advanced photocatalytic materials with g-C_3N_4, and the above

challenges must be able to overcome in the near future. To sum up, the prospect of photocatalytic disinfection looks bright. In the near future, it is sure that nanocomposites based on g-C_3N_4 will have many interesting opportunities in this field, which requires the joint efforts of scientists worldwide.

Acknowledgements

This study was financially supported by the Program for the National Program for Support of Top-Notch Young Professionals of China (2014), the National Natural Science Foundation of China (51521006, 51879101, 51809090, 51579098, 51779090, 51709101, 51709100, 51278176, 51378190, 51408206, 51909084), the Fundamental Research Funds for the Central Universities, Hunan Provincial Science and Technology Plan Project (No.2016RS3026, 2017SK2243, 2018SK20410), the Three Gorges Follow-up Research Project (2017HXXY-05), the Program for New Century Excellent Talents in University (NCET-13-0186), the Natural Science Foundation of Hunan Province, China (Grant Nos. 2019JJ50077), the Fundamental Research Funds for the Central Universities (531119200086, 531118010114, 531107050978, 541109060031), and the Program for Changjiang Scholars and Innovative Research Team in University (IRT-13R17).

.

Table 1. Photocatalytic disinfection of g-C_3N_4 with different nanostructures and surface modification.

Photocatalyst	Nanostructure	Target microorganism and microbial level (CFU/mL)	Light source	Inactivation performance	Time (h)	Catalyst dose (g/L)	Ref (year)
PCNS	porous nanosheet	*E. coli* 5×10^6	500 W xenon lamp with a 420 nm cutoff filter	6.7-log	4	0.4	[41] 2017
g-C_3N_4	mesoporous	*E. coli* K-12 2.5×10^6	300 W Xenon lamp with a 420 nm cutoff filter	6.39-log	4	1	[42] 2014
BT-CN	nanosheets	*E. coli* 3×10^7	300 W Xenon lamp with a 420 nm cutoff filter	7.47-log	2	1	[43] 2018
F-g-C_3N_4-30-EP	nanosheets	*E. coli* 1×10^6	300 W Xenon lamp with a 400 nm cutoff filter	6-log	0.5	0.01	[46] 2019
SL g-C_3N_4	single layer nanosheet	*E. coli* 2×10^7	500 W xenon lamp with a 400 nm cutoff filter	7.3-log	4	0.1	[47] 2014
CNCT	core shell	*E. coli* 1×10^6	300 W Xenon lamp with a 420 nm cutoff filter	6-log	1.2	0.5	[54] 2020
HTCN	hollow tubular	*E. coli* 3×10^9	300 W Xenon lamp with a 420 nm cutoff filter	2.36-log	0.67	0.6	[57] 2019

O-g-C_3N_4	doping	*HAdV-2* 1×10^5	7 W-white light emitting diode lamp ($\lambda > 400$ nm)	1.5-log	2	0.15	[64] 2019
Ag/PSCN	co-doping	*E. coli* 1×10^7	300 W Xenon lamp with a 420 nm cutoff filter	7-log	1	0.5	[68] 2020
CN-4	nanosheet with nitrogen defects	*E. coli* and *S. aureus* 1×10^6	300 W Xenon lamp with a 420 nm cutoff filter	4.80-log 4.24-log	2	4	[75] 2020
Ag/g-C_3N_4	noble metals	*E. coli* 1×10^7	300 W Xenon lamp with a 420 nm cutoff filter	7-log	1.5	4	[82] 2016
Ag/PCNO	noble metals	*S. aureus* 1×10^7	500 W Xenon lamp with a 420 nm cutoff filter	7-log	4	0.2	[84] 2019
g-C_3N_4	bulk	*Bacteriophage MS2* 1×10^8	300 W Xenon lamp with a 400 nm cutoff filter	8-log	6	N/A	[141] 2016

Table 2. Photocatalytic disinfection of g-C_3N_4 heterojunction.

Photocatalyst	Heterojunction	Target microorganism and microbial level (CFU/mL)	Light source	Inactivation performance	Time (h)	Catalyst dose (g/L)	Ref
HTCN-C(2)	CQDs/ tubular g-C_3N_4	*E. coli* 1×10^7	300 W Xenon lamp with a 420 nm cutoff filter	6.88-log	0.67	1	[57] 2019
CNP	g-C_3N_4/red P	*E. coli* K-12 1×10^7	300 W Xenon lamp with a 420 nm cutoff filter	7-log	1.34	1	[63] 2018
$CNRGOS_8$	g-C_3N_4/RGO	*E. coli* K-12 2×10^6	300 W Xenon lamp with a 400 nm cutoff filter	6.3-log	4	N/A	[91] 2013
GO/g-C_3N_4	GO/g-C_3N_4	*E. coli* 1×10^7	300 W Xenon lamp with a 420 nm cutoff filter	6.99-log	2	0.1	[94] 2017
fullerene/C_3N_4	C_{60}/g-C_3N_4 C_{70}/g-C_3N_4	*E. coli* O157:H7 3×10^8	300 W Xenon lamp with a 420 nm cutoff filter	8.4-log 8.47-log	4	0.5	[95] 2017
vanadate QDs/g-C_3N_4,	$AgVO_3$/g-C_3N_4 $BiVO_3$/g-C_3N_4	*Salmonella* H9812 1×10^7	300 W Xenon lamp with a 400 nm cutoff filter	6.93-log 6.97-log	0.5	0.75	[96] 2018
TiO_2/g-C_3N_4	TiO_2/g-C_3N_4	*E. coli* K-12 1×10^7	300 W Xenon lamp with a 420 nm cutoff filter	7-log	3	0.6	[102] 2015

MnO_2/g-C_3N_4	MnO_2/g-C_3N_4	*E. coli* and *S. aureus* 1×10^5	300 W Xenon lamp with a 420 nm cutoff filter	4.98-log 4.99-log	0.34	N/A	[103] 2019
TiNT/g-C_3N_4	TiO_2/g-C_3N_4	*E. coli* DH5α 1×10^5	300 W Xenon lamp with a 420 nm cutoff filter	4.92-log	3	N/A	[104] 2016
ZnO/g-C_3N_4	ZnO/g-C_3N_4	*E. coli* and *S. aureus* 1×10^8	300 W Xenon lamp with a 420 nm cutoff filter	7.77-log 7.95-log	1	0.1	[105] 2017
$MgTi_2O_5$/g-C_3N_4	$MgTi_2O_5$/g-C_3N_4	*E. coli* 1×10^7	300 W Xenon lamp with a 400 nm cutoff filter	7.4-log	3	0.5	[106] 2019
Ag_2WO_4/g-C_3N_4	Ag_2WO_4/g-C_3N_4	*E. coli* 1×10^9	300 W Xenon lamp with a 420 nm cutoff filter	9-log	1.5	0.1	[107] 2017
EP/g-C_3N_4	EP/g-C_3N_4	*E. coli* and *MS2 phage* 1×10^8	300 W Xenon lamp with a 400 nm cutoff filter	8-log 8-log	3 4	N/A	[111] 2018
Bi_2MoO_6/g-C_3N_4	Bi_2MoO_6/g-C_3N_4	*E. coli* 2.5×10^7	300 W Xenon lamp with a 420 nm cutoff filter	6-log	2.5	0.1	[118] 2017
BiOBr/g-C_3N_4	BiOBr/g-C_3N_4	*E. coli* CICC 10389 1×10^6	300 W Xenon lamp with a 400 nm cutoff filter	5.91-log	2	N/A	[120] 2019
m-Bi_2O_4/g-C_3N_4	m-Bi_2O_4/g-C_3N_4	*E. coli* K-12	300 W Xenon lamp with a	6-log	1.5	0.4	[121]

		1×10^6	400 nm cutoff filter				2017
$g\text{-}C_3N_4/Ag/BiVO_4$	$g\text{-}C_3N_4/Ag/BiVO_4$	*E. coli* K-12	Philips Mini 8W E14 Cool	6.5-log	1	0.1	[126]
		3×10^6	Daylight, Netherlands				2019
$g\text{-}C_3N_4/TiO_2/$	$g\text{-}C_3N_4/TiO_2/$	*Microcystis aeruginosa*	500 W Xenon lamp with a	6.35-log	6	2	[130]
Al_2O_3/EP	Al_2O_3/EP	2.7×10^6	400 nm cutoff filter				2018
$g\text{-}C_3N_4/BiOI/BiOBr$	$g\text{-}C_3N_4/BiOI/BiOBr$	*E. coli* ATCC 15597	300 W Xenon lamp with a	3-log	3	0.5	[132]
		1×10^3	400 nm cutoff filter				2018
$AgBr/g\text{-}C_3N_4$	$AgBr/g\text{-}C_3N_4$	*E. coli* and *S. aureus*	300 W Xenon lamp with a	6.47-log	1	0.1	[171]
		3×10^6	420 nm cutoff filter	6.47-log	2.5		2017
$Ni_2P/g\text{-}C_3N_4$	$Ni_2P/g\text{-}C_3N_4$	*E. coli* K-12	300 W Xenon lamp with a	7-log	4	1	[176]
		1×10^7	420 nm cutoff filter				2017

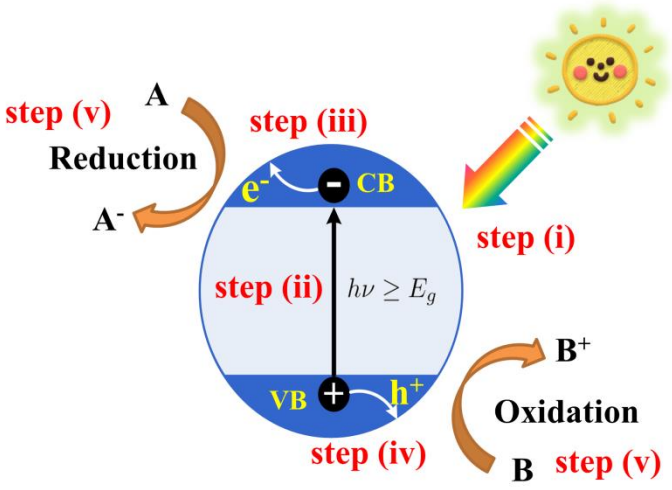

Fig. 1. Typical five steps in the photocatalytic reaction process of semiconductor.

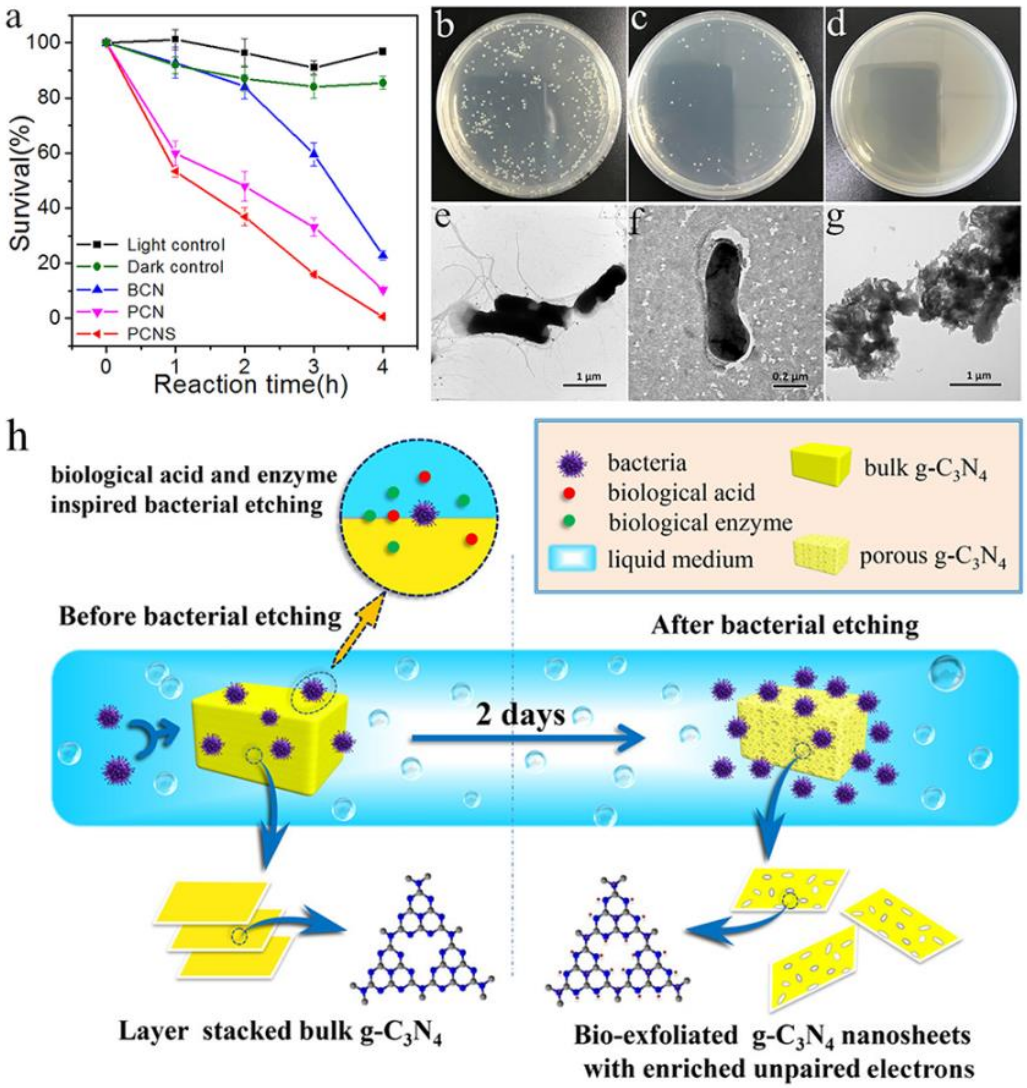

Fig. 2. (a) VLD photocatalytic disinfection performance against *E. coli* over BCN, PCN, and PCNS. Images of *E. coli* colonies on solid culture medium (b) before irradiation and (c) after disinfection for 2 h and (d) for 4 h using PCNS. TEM images of *E. coli* cells (e) before irradiation and (f, g) after disinfection for 4 h using PCNS. ((a-g) are reprinted with permission from Ref. [41]. Copyright 2017 American Chemical Society; (h) is reprinted with permission from Ref. [43]. Copyright 2018 American Chemical Society.)

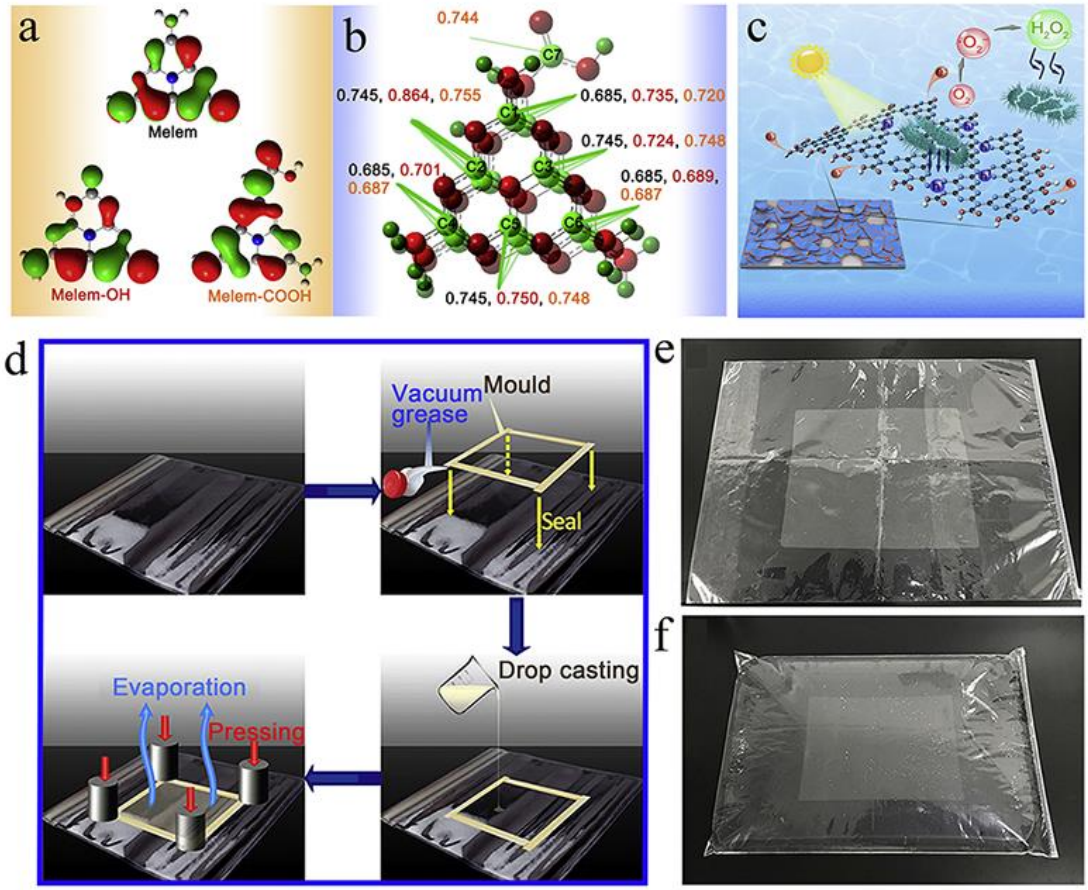

Fig. 3. (a) Highest occupied molecular orbitals of $Melem^+$, $Melem\text{-}OH^+$, and $Melem\text{-}COOH^+$; (b) Mulliken charge distribution of different carbon atoms in $Melem^+$ (black numbers), $Melem\text{-}OH^+$ (red numbers), and $Melem\text{-}COOH^+$ (orange numbers); (c) Schematic diagram of indirect bacteria inactivation using H_2O_2 generated by an edge-functionalized g-C_3N_4 nanosheet; (d) Diagrammatic sketch of the modification process utilizing F-g-C_3N_4-30-EP coated onto a polyethylene bag modified by a silane coupling agent. (e) Photograph of newly prepared F-g-C_3N_4-30-EP-modified polyethylene bags. (f) Photograph of newly prepared F-g-C_3N_4-30-EP-modified polyethylene bag filled with water. (Reprinted with permission from Ref. [46]. Copyright 2019 Cell.)

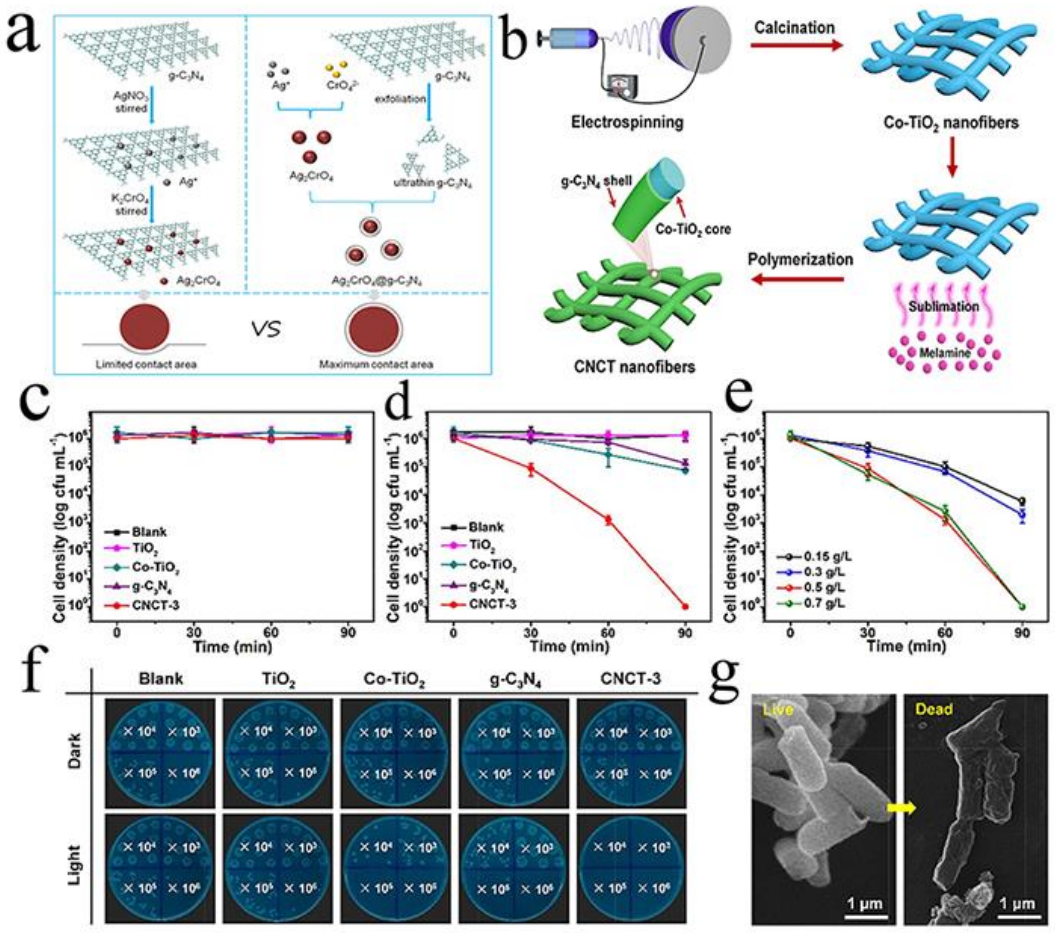

Fig. 4. (a) The schematic diagram of combinations of Ag_2CrO_4 and g-C_3N_4. The growth of Ag_2CrO_4 nanoparticle on the surface of g-C_3N_4 obtain limited contact area, and the core-shell Ag_2CrO_4@g-C_3N_4 provide the maximum contact area; (b) Schematic illustration for the fabrication of soft CNCT nanofibrous membranes; And disinfection efficiency against *E. coil* over blank, TiO_2, Co-TiO_2, g-C_3N_4, and CNCT-3 (c) in the dark and (d) under visible light irradiation; (e) Effect of CNCT-3 dosage on the photocatalytic inactivation of *E. coil*; (f) Photographs of *E. coil* colonies treated by different photocatalysts without and with visible light irradiation for 90 min, respectively; (g) SEM images of *E. coil* cells before (left) and after (right) photocatalytic disinfection using CNCT-3 membrane. ((a) is reprinted with permission from Ref. [53]. Copyright 2018 Elsevier; (b-g) are reprinted with permission from Ref. [54]. Copyright 2020 Elsevier.)

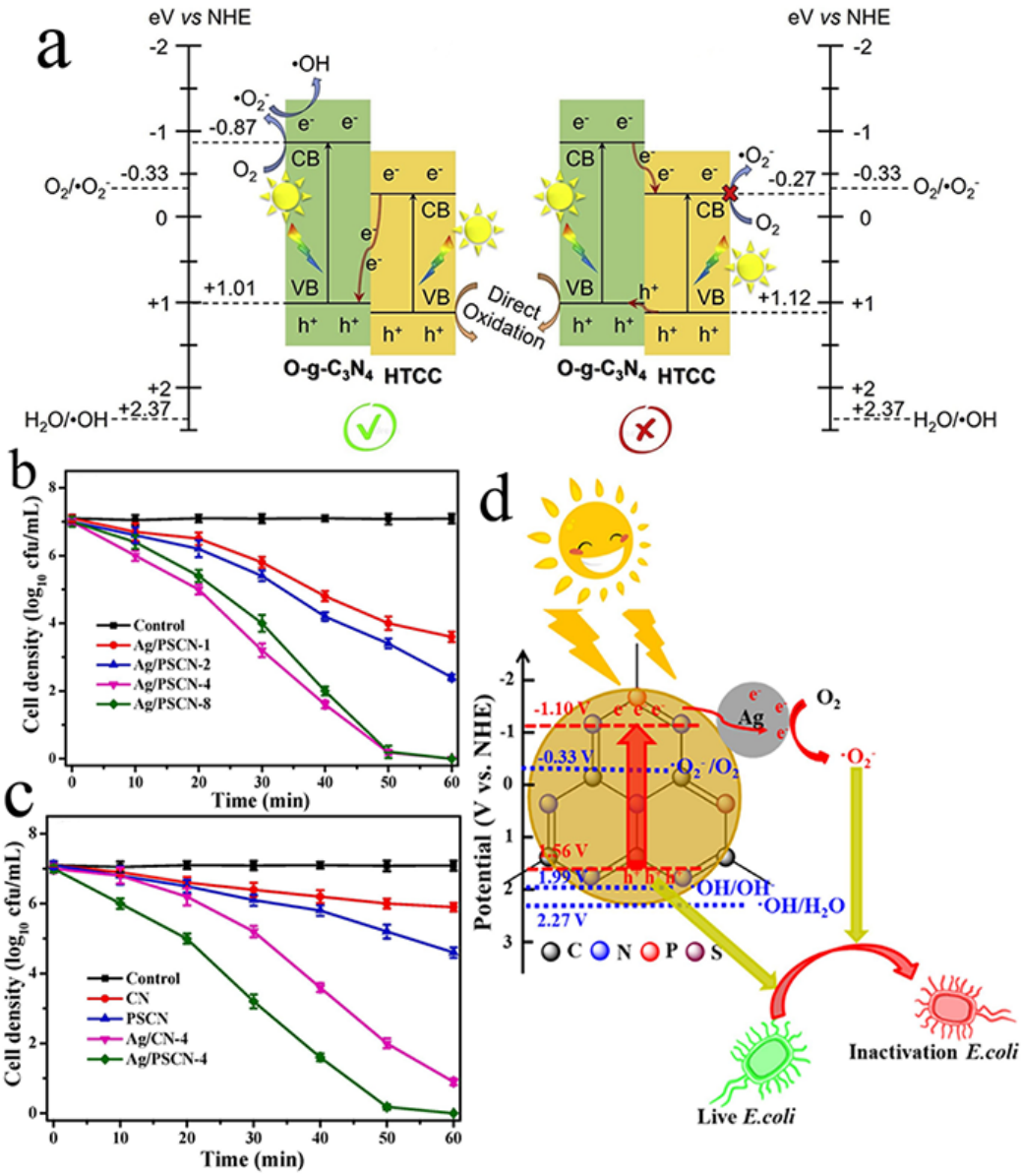

Fig. 5. (a) Two possible heterojunctions of Z-scheme and Type II proposed for O-g-C_3N_4/HTCC-2 in photocatalysis; Photocatalytic inactivation towards *E. coli* under visible light irradiation: with Ag/PSCN (b) and with different as-prepared composites (c); (d) Photocatalytic inactivation mechanism of Ag/PSCN-4 under visible light irradiation. ((a) is reprinted with permission from Ref. [64]. Copyright 2019 Elsevier. (b-d) are reprinted with permission from Ref. [68]. Copyright 2020 Elsevier.)

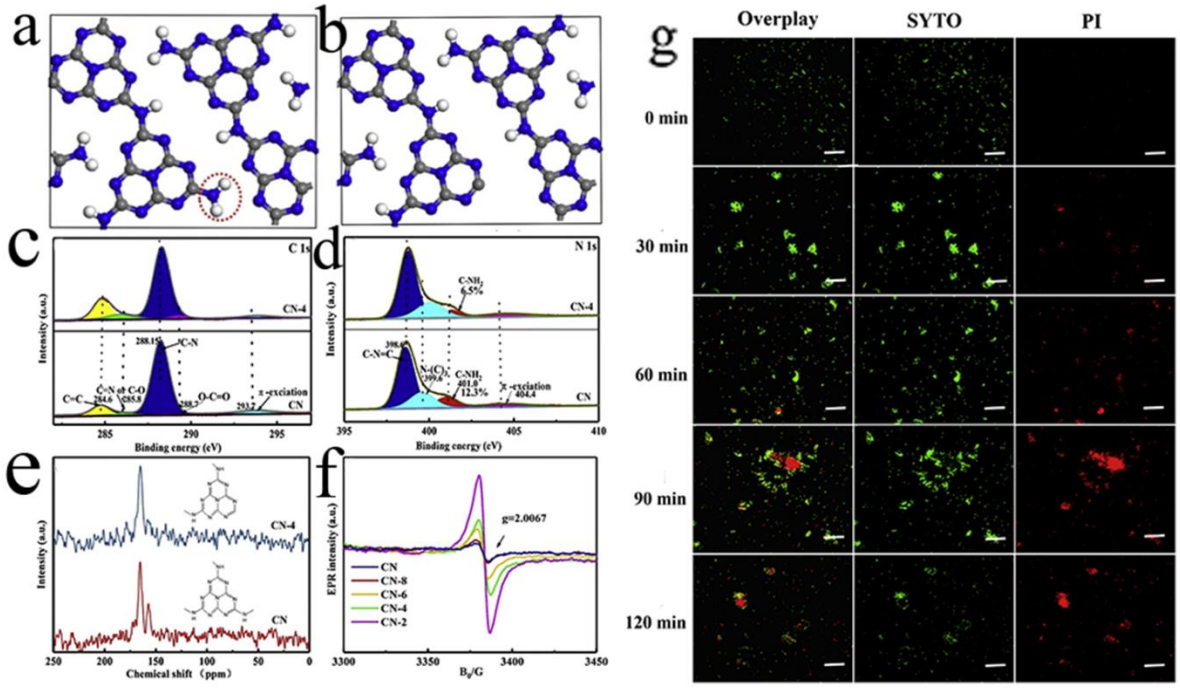

Fig. 6. Top view of the optimized (a) CN and (b) CN-4 configuration, color scheme: C, grey; N, blue; H, white; The XPS spectra of (c) C 1s, (d) N 1s and (e) solidstate ^{13}C MAS NMR spectra of the CN and CN-4 (the insets are their tri-s-triazine rings); (f) room-temperature EPR spectra of the CN, CN-8, CN-6, CN-4, CN-2; (g) Confocal fluorescent images of live and dead E. coli (10^9 cfu/mL) treated with 100 mg/L of CN-4 under visible light irradiation. The scale bar is 50 μm. (Reprinted with permission from Ref. [75]. Copyright 2020 Elsevier.)

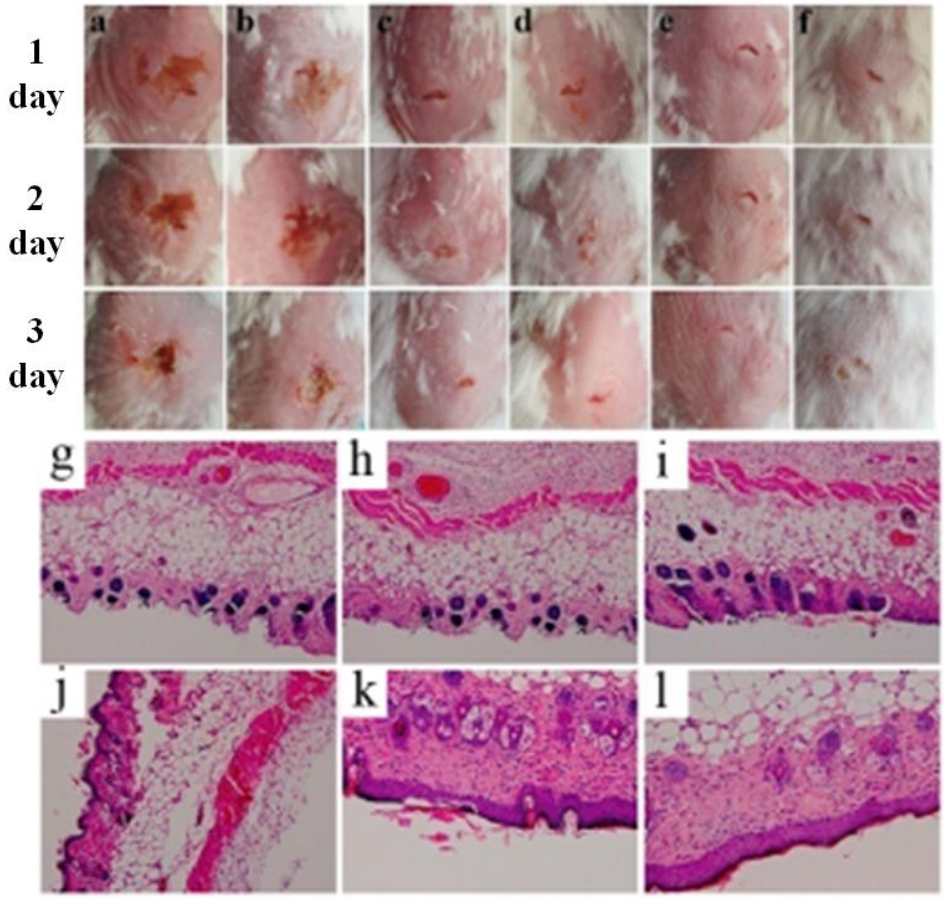

Fig. 7. Photographs of wound on the mice from the six groups at different times during the therapeutic process. Please note that in all these statistics (a) control; (b) g-C_3N_4(20 μg/mL); (c) CNA (20 μg/mL); (d) H_2O_2 (100 μM); (e) g-C_3N_4 (20 μg/mL) + H_2O_2 (100 μM); (f) CNA (20 mg/mL) + H_2O_2 (100 μM); Photomicrographs showing section of skin tissues with H&E staining. (g) control; (h) g-C_3N_4; (i) CNA; (j) H_2O_2; (k) g-C_3N_4 + H_2O_2; (l) CNA + H_2O_2. All fluorescence images were obtained under magnification of 20. (Reprinted with permission from Ref. [85]. Copyright 2017 Elsevier.)

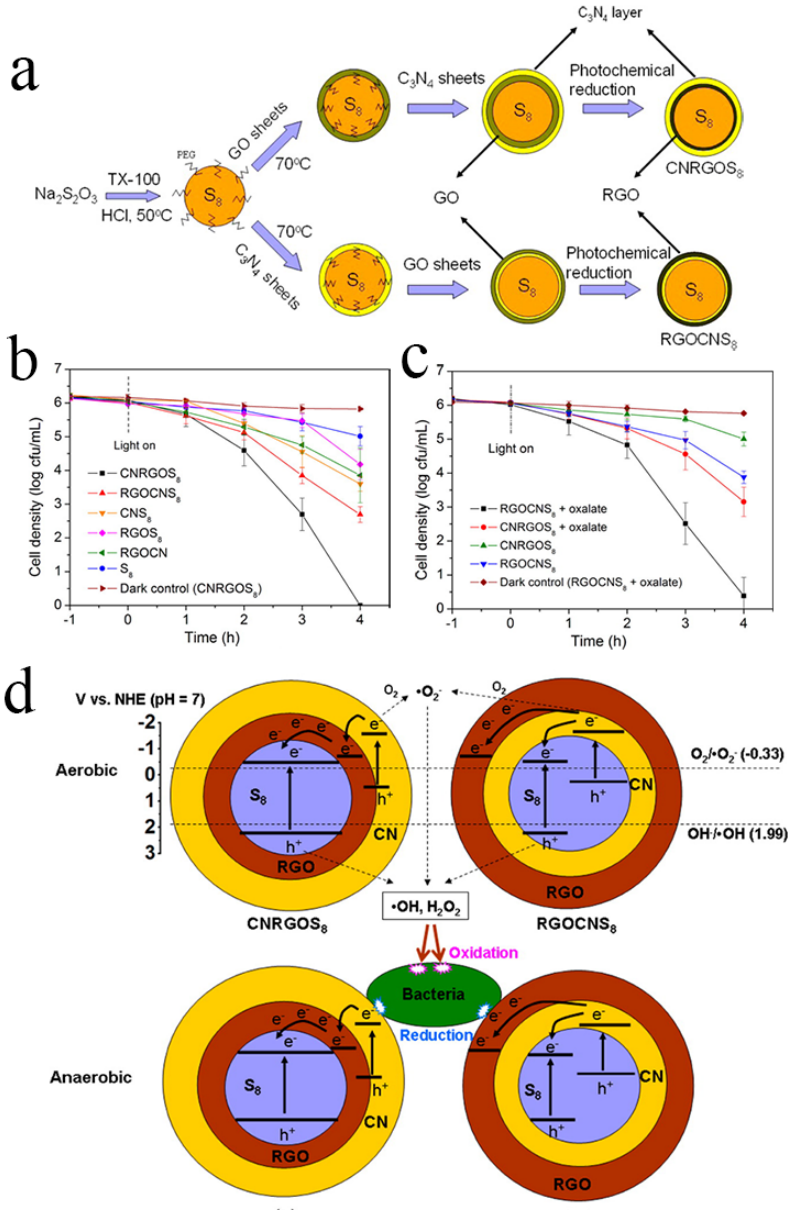

Fig. 8. (a) Schematic illustration of the two different synthetic pathways for the praparation of graphene and C_3N_4 sheets cowrapped α-sulfur; Photocatalytic inactivation efficiency against *E. coli* K-12 (2×10^6 cfu/mL, 50 mL) in the presence of the as-prepared samples in aerobic (b) and anaerobic (c) condition under visible light irradiation. No inactivation occurs in the dark and light controls; (d) Schematic illustration of the VLD photocatalytic bacterial inactivation mechanisms of CNRGOS8 andRGOCNS8 in aerobic condition, and CNRGOS8 and RGOCNS8 in anaerobic condition. (Reprinted with permission from Ref. [91]. Copyright 2013 American Chemical Society.)

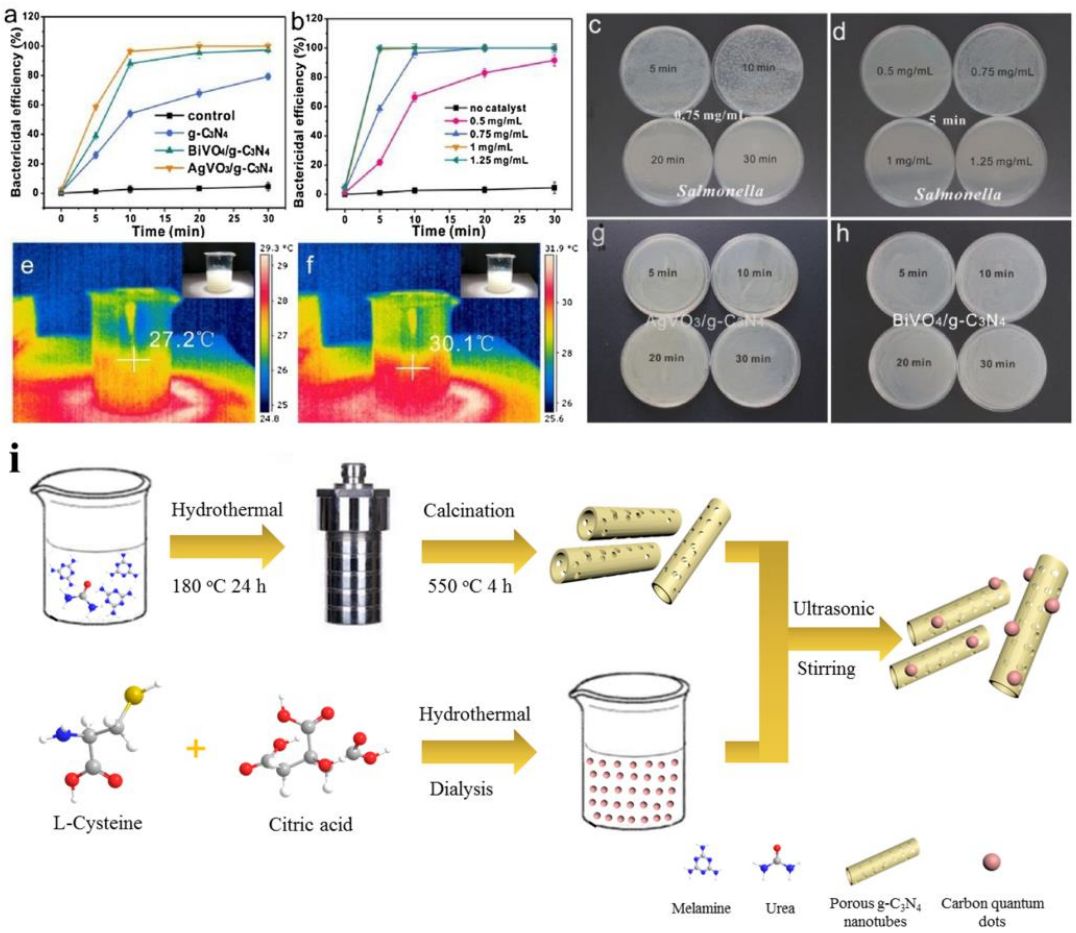

Fig. 9. (a) Bactericidal efficiency against Salmonella with different samples under concentration of 0.75 mg/mL; (b) Bactericidal efficiency against *Salmonella* with $AgVO_3$/g-C_3N_4 under different concentrations; (c) Bacterial colony growth in the presence of $AgVO_3$/g-C_3N_4 with Salmonella; (d) Bacterial colony growth in the presence of $AgVO_3$/g-C_3N_4 with *Salmonella* under different concentrations; The corresponding thermal images of $AgVO_3$/g-C_3N_4 at (e) 5 min and (f) 30 min irradiation; Bacterial colony growth with (g) $AgVO_3$/g-C_3N_4 and (h) $BiVO_4$/g-C_3N_4 in the dark; (i) Schematic illustration of the preparation for modifed carbon quantum dots loaded hollow tubular carbon nitride (HTCN-C) samples. ((a-h) are reprinted with permission from Ref. [96]. Copyright 2018 Elsevier. (i) is reprinted with permission from Ref. [57]. Copyright 2020 Elsevier.)

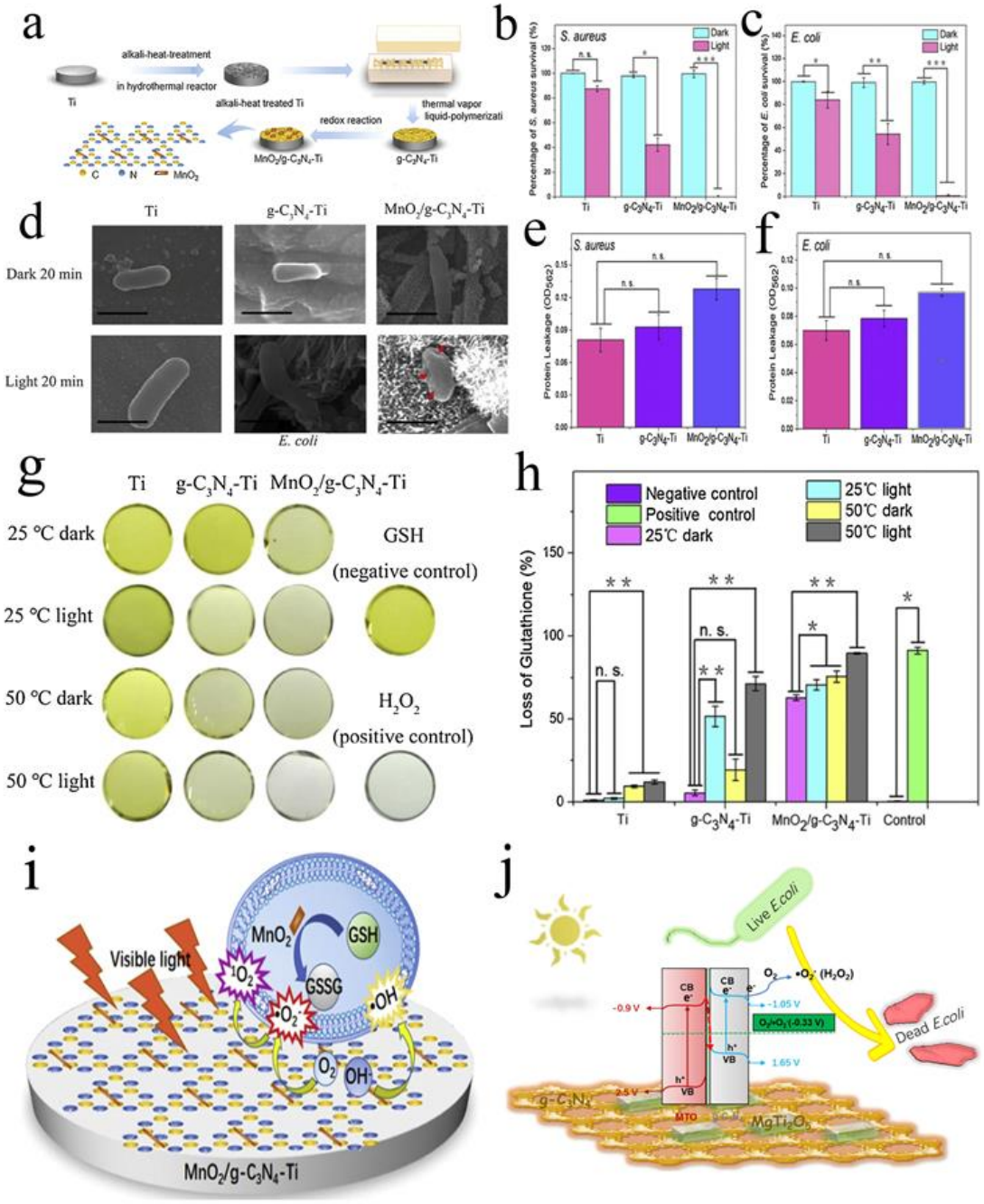

Fig. 10. (a) The procedure of synthesizing MnO_2/g-C_3N_4-Ti; The antibacterial effect of as-prepared samples on (b) *S. aureus*, and (c) *E. coli* after irradiation for 20 min; the antibacterial effect of samples on (d) SEM morphology of *E. coli* after irradiation or dark treatment for 20 min (scale bars = 1 μm); Various samples under illumination caused the protein leakage toward (e) *S. aureus* and (f) *E. coli* after irradiation for 20 min. (g)The color change of GSH solution treated with samples in diverse conditions, and (h) the corresponding loss plot of GSH; The error bars indicate means ± standard

deviations: *P < 0.05, **P < 0.01, ***P < 0.001, n. s. means no significance; (i) schematic illustrating the mechanism of the antibacterial property of MnO_2/g-C_3N_4-Ti under visible light; (j) Proposed mechanism for the photocatalytic inactivation toward *E. coli* by Z-scheme $MgTi_2O_5$/g-C_3N_4 composite. ((a-i) are reprinted with permission from Ref. [103]. Copyright 2019 Elsevier. (j) is reprinted with permission from Ref. [106]. Copyright 2019 Elsevier.)

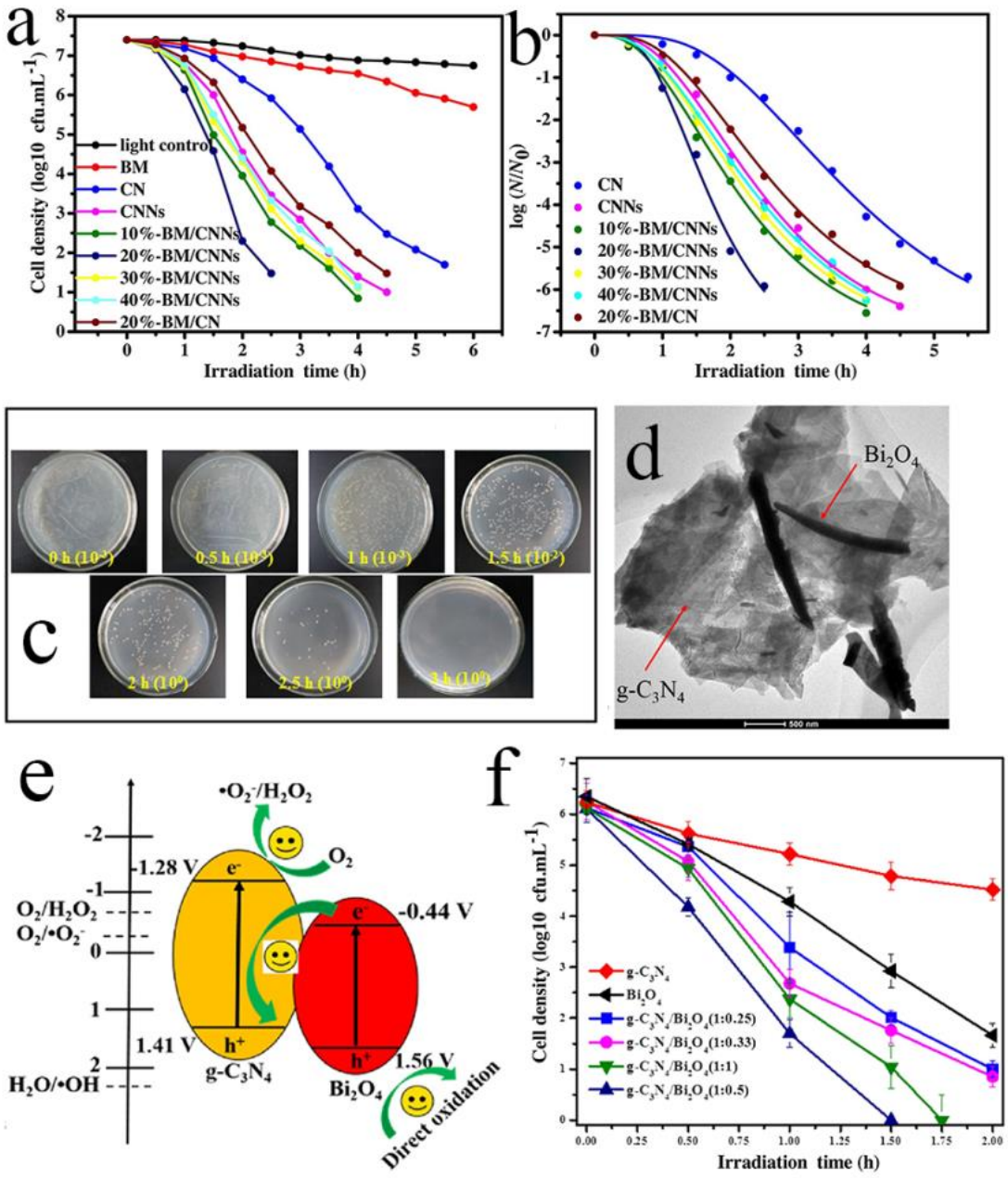

Fig. 11. (a) Photocatalytic disinfection efficiency of *E. coli* for different samples; (b) Fitted curves of photocatalytic disinfection using modified Hom model; (c) Bacterial colonies of re-cultured *E. coli* after dealing with 20%-BM/CNNs at different time and dilution multiple; (d) TEM image of m-Bi_2O_4-g-C_3N_4; (e) Z-scheme electron transfer model for m-Bi_2O_4-g-C_3N_4; (f) photocatalytic inactivation of *E. coli* by m-Bi_2O_4, m-Bi_2O_4-g-C_3N_4 and g-C_3N_4. ((a-c) are reprinted with permission from Ref. [118]. Copyright 2017 Elsevier. (d-f) are reprinted with permission from Ref. [121]. Copyright 2017 Elsevier.)

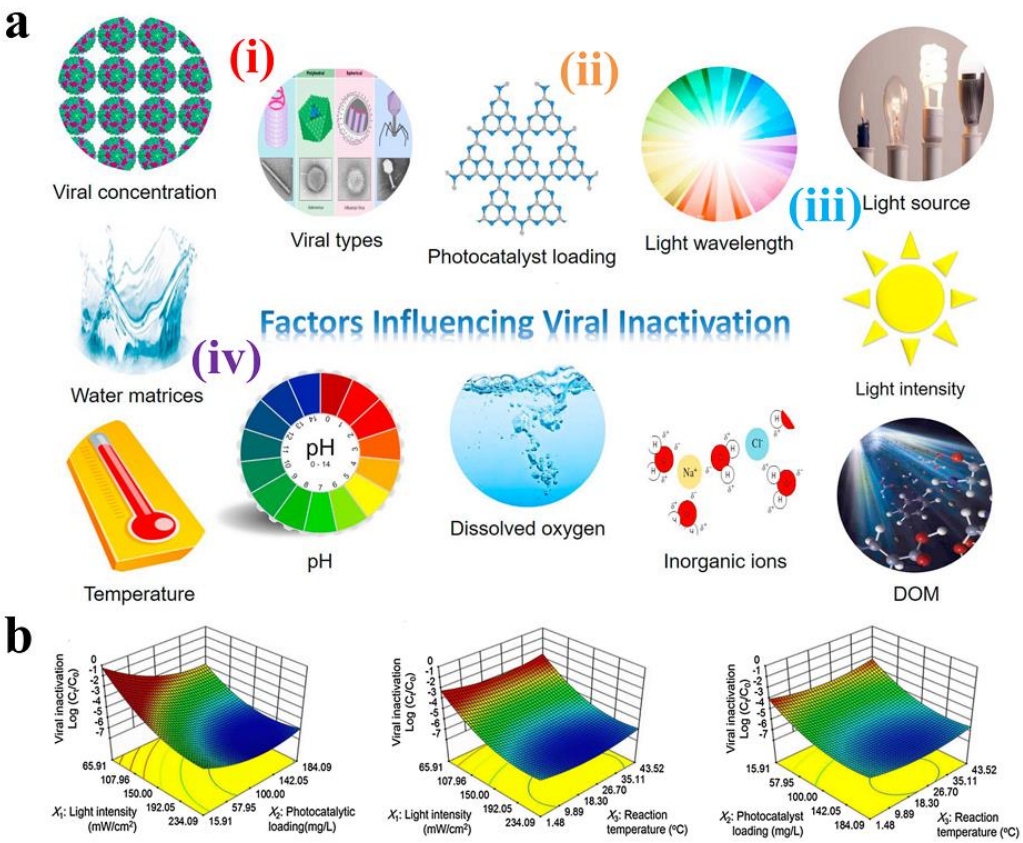

Fig. 12. (a) Various factors influencing photocatalytic viral disinfection with minor modifications from Ref. [142]. Copyright 2019 Elsevier. (b) The 3D response surface plots of the photocatalytic viral inactivation efficiency by g-C_3N_4. Reprinted with permission from Ref. [10]. Copyright 2018 Elsevier.

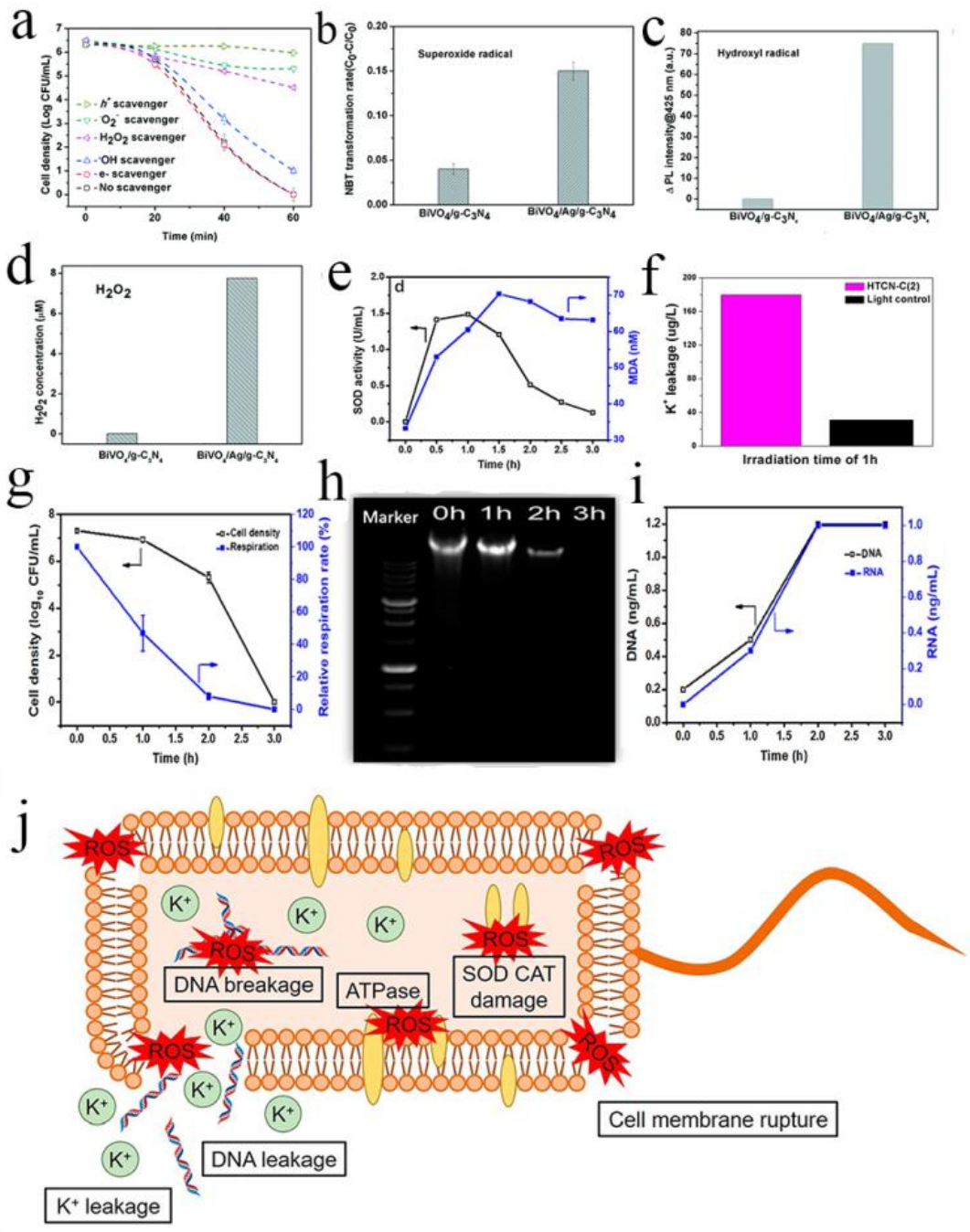

Fig. 13. (a) Effect of reactive species scavengers on the disinfection activity of $BiVO_4$/Ag/g-C_3N_4; Transformation percentage of NBT concentration (b), changes of fluorescence intensity at 425 nm (c) and the concentration of H_2O_2 produced (d) by $BiVO_4$/g-C_3N_4 and $BiVO_4$/Ag/g-C_3N_4 after 1 h of visible light irradiation; (e) MDA generation and SOD activity during the photocatalytic disinfection of *E. coli*; (f) Leakage of K^+ from *E. coli* cells under visible light irradiation; (g) Cell density and relative respiration activity; (h) Investigation of the leakage bacterial genomic DNA

extracted from harvested cells; (i) Concentration of the leakage of DNA and RNA during the destruction of bacterial cells; (j) Responses of bacterial to g-C_3N_4-based photocatalytic disinfection. ((a-d) are reprinted with permission from Ref. [126]. Copyright 2019 Royal Society of Chemistry. (e and g-i) are reprinted with permission from Ref. [106]. Copyright 2019 Elsevier. (f) is reprinted with permission from Ref. [57]. Copyright 2019 Elsevier. (j) is reprinted with permission from Ref. [156]. Copyright 2019 Elsevier.

[1] S. Loeb, R. Hofmann, J.-H. Kim, Beyond the pipeline: Assessing the efficiency limits of advanced technologies for solar water disinfection, Environmental Science & Technology Letters 3 (2016) 73-80.
[2] M.A. Shannon, P.W. Bohn, M. Elimelech, J.G. Georgiadis, B.J. Marinas, A.M. Mayes, Science and technology for water purification in the coming decades, Nanoscience and technology: a collection of reviews from nature Journals, World Scientific2010, pp. 337-346.
[3] C. Zhang, G. Zeng, D. Huang, C. Lai, M. Chen, M. Cheng, W. Tang, L. Tang, H. Dong, B. Huang, X. Tan, R. Wang, Biochar for environmental management: Mitigating greenhouse gas emissions, contaminant treatment, and potential negative impacts, Chemical Engineering Journal 373 (2019) 902-922.
[4] H. Wang, Z. Zeng, P. Xu, L. Li, G. Zeng, R. Xiao, Z. Tang, D. Huang, L. Tang, C. Lai, Recent progress in covalent organic framework thin films: fabrications, applications and perspectives, Chemical Society reviews 48 (2019) 488-516.
[5] B.E. Logan, M. Elimelech, Membrane-based processes for sustainable power generation using water, Nature 488 (2012) 313.
[6] H. Yang, S. Ye, Z. Zeng, G. Zeng, X. Tan, R. Xiao, J. Wang, B. Song, L. Du, M. Qin, Y. Yang, F. Xu, Utilization of biochar for resource recovery from water: A review, Chemical Engineering Journal 397 (2020) 125502.
[7] S. Ye, M. Cheng, G. Zeng, X. Tan, H. Wu, J. Liang, M. Shen, B. Song, J. Liu, H. Yang, Y. Zhang, Insights into catalytic removal and separation of attached metals from natural-aged microplastics by magnetic biochar activating oxidation process, Water research 179 (2020).
[8] W.-Y. Huang, Z.-Q. Shen, J.-Z. Cheng, L.-L. Liu, K. Yang, X. Chen, H.-R. Wen, S.-Y. Liu, C–H activation derived CPPs for photocatalytic hydrogen production excellently accelerated by a DMF cosolvent, Journal of Materials Chemistry A 7 (2019) 24222-24230.
[9] M.A. Montgomery, M. Elimelech, Water And Sanitation in Developing Countries: Including Health in the Equation, Environmental Science & Technology 41 (2007) 17-24.
[10] C. Zhang, Y. Li, W. Zhang, P. Wang, C. Wang, Metal-free virucidal effects induced by g-C3N4 under visible light irradiation: Statistical analysis and parameter optimization, Chemosphere 195 (2018) 551-558.
[11] L. Qin, Z. Zeng, G. Zeng, C. Lai, A. Duan, R. Xiao, D. Huang, Y. Fu, H. Yi, B. Li, Cooperative catalytic performance of bimetallic Ni-Au nanocatalyst for highly efficient hydrogenation of nitroaromatics and corresponding mechanism insight, Applied Catalysis B: Environmental 259 (2019) 118035.
[12] Y. Liu, G. Zeng, H. Zhong, Z. Wang, Z. Liu, M. Cheng, G. Liu, X. Yang, S. Liu, Effect of rhamnolipid solubilization on hexadecane bioavailability: enhancement or reduction?, Journal of hazardous

materials 322 (2017) 394-401.
[13] C. Zhang, C. Lai, G. Zeng, D. Huang, C. Yang, Y. Wang, Y. Zhou, M. Cheng, Efficacy of carbonaceous nanocomposites for sorbing ionizable antibiotic sulfamethazine from aqueous solution, Water research 95 (2016) 103-112.
[14] Y. Yang, Z. Zeng, C. Zhang, D. Huang, G. Zeng, R. Xiao, C. Lai, C. Zhou, H. Guo, W. Xue, M. Cheng, W. Wang, J. Wang, Construction of iodine vacancy-rich BiOI/Ag@AgI Z-scheme heterojunction photocatalysts for visible-light-driven tetracycline degradation: Transformation pathways and mechanism insight, Chemical Engineering Journal 349 (2018) 808-821.
[15] X. Li, Z. Zeng, G. Zeng, D. Wang, R. Xiao, Y. Wang, C. Zhou, H. Yi, S. Ye, Y. Yang, W. Xiong, A “bottle-around-ship” like method synthesized yolk-shell Ag3PO4@MIL-53(Fe) Z-scheme photocatalysts for enhanced tetracycline removal, Journal of colloid and interface science 561 (2020) 501-511.
[16] J. Cao, S. Sun, X. Li, Z. Yang, W. Xiong, Y. Wu, M. Jia, Y. Zhou, C. Zhou, Y. Zhang, Efficient charge transfer in aluminum-cobalt layered double hydroxide derived from Co-ZIF for enhanced catalytic degradation of tetracycline through peroxymonosulfate activation, Chemical Engineering Journal 382 (2020) 122802.
[17] J.-Z. Cheng, L.-L. Liu, G. Liao, Z.-Q. Shen, Z.-R. Tan, Y.-Q. Xing, X.-X. Li, K. Yang, L. Chen, S.-Y. Liu, Achieving an unprecedented hydrogen evolution rate by solvent-exfoliated CPP-based photocatalysts, Journal of Materials Chemistry A 8 (2020) 5890-5899.
[18] F. Ding, D. Yang, Z. Tong, Y. Nan, Y. Wang, X. Zou, Z. Jiang, Graphitic carbon nitride-based nanocomposites as visible-light driven photocatalysts for environmental purification, Environmental Science: Nano 4 (2017) 1455-1469.
[19] H. Guo, H.-Y. Niu, C. Liang, C.-G. Niu, D.-W. Huang, L. Zhang, N. Tang, Y. Yang, C.-Y. Feng, G.-M. Zeng, Insight into the energy band alignment of magnetically separable Ag2O/ZnFe2O4 pn heterostructure with rapid charge transfer assisted visible light photocatalysis, Journal of Catalysis 370 (2019) 289-303.
[20] Y. Yang, G. Zeng, D. Huang, C. Zhang, D. He, C. Zhou, W. Wang, W. Xiong, X. Li, B. Li, Molecular engineering of polymeric carbon nitride for highly efficient photocatalytic oxytetracycline degradation and H2O2 production, Applied Catalysis B: Environmental (2020) 118970.
[21] T. Matsunaga, R. Tomoda, T. Nakajima, H. Wake, Photoelectrochemical sterilization of microbial cells by semiconductor powders, FEMS Microbiology Letters 29 (1985) 211-214.
[22] W. Wang, G. Li, D. Xia, T. An, H. Zhao, P.K. Wong, Photocatalytic nanomaterials for solar-driven bacterial inactivation: recent progress and challenges, Environmental Science: Nano 4 (2017) 782-799.
[23] S. Ye, M. Yan, X. Tan, J. Liang, G. Zeng, H. Wu, B. Song, C. Zhou, Y. Yang, H. Wang, Facile assembled biochar-based nanocomposite with improved graphitization for efficient photocatalytic activity driven by visible light, Applied Catalysis B: Environmental 250 (2019) 78-88.
[24] X. Chen, S.S. Mao, Titanium dioxide nanomaterials: synthesis, properties, modifications, and applications, Chemical reviews 107 (2007) 2891-2959.
[25] H. Yi, M. Li, X. Huo, G. Zeng, C. Lai, D. Huang, Z. An, L. Qin, X. Liu, B. Li, Recent development of advanced biotechnology for wastewater treatment, Critical reviews in biotechnology 40 (2020) 99-118.
[26] H. Guo, C.-G. Niu, C.-Y. Feng, C. Liang, L. Zhang, X.-J. Wen, Y. Yang, H.-Y. Liu, L. Li, L.-S. Lin, Steering exciton dissociation and charge migration in green synthetic oxygen-substituted ultrathin porous graphitic carbon nitride for boosted photocatalytic reactive oxygen species generation, Chemical Engineering Journal 385 (2020) 123919.

[27] Z. Zhu, C. Ma, K. Yu, Z. Lu, Z. Liu, P. Huo, X. Tang, Y. Yan, Synthesis Ce-doped biomass carbon-based g-C3N4 via plant growing guide and temperature-programmed technique for degrading 2-Mercaptobenzothiazole, Applied Catalysis B: Environmental (2019) 118432.
[28] L.-S. Lin, Z.-X. Cong, J. Li, K.-M. Ke, S.-S. Guo, H.-H. Yang, G.-N. Chen, Graphitic-phase C3N4 nanosheets as efficient photosensitizers and pH-responsive drug nanocarriers for cancer imaging and therapy, Journal of Materials Chemistry B 2 (2014) 1031.
[29] H. Yi, M. Yan, D. Huang, G. Zeng, C. Lai, M. Li, X. Huo, L. Qin, S. Liu, X. Liu, Synergistic effect of artificial enzyme and 2D nano-structured Bi2WO6 for eco-friendly and efficient biomimetic photocatalysis, Applied Catalysis B: Environmental 250 (2019) 52-62.
[30] Y. Li, X. Liu, L. Tan, Z. Cui, X. Yang, Y. Zheng, K.W.K. Yeung, P.K. Chu, S. Wu, Rapid Sterilization and Accelerated Wound Healing Using Zn2+
and Graphene Oxide Modified g-C3
N4
under Dual Light Irradiation, Advanced Functional Materials 28 (2018) 1800299.
[31] C. Mao, Y. Xiang, X. Liu, Z. Cui, X. Yang, Z. Li, S. Zhu, Y. Zheng, K.W.K. Yeung, S. Wu, Repeatable Photodynamic Therapy with Triggered Signaling Pathways of Fibroblast Cell Proliferation and Differentiation To Promote Bacteria-Accompanied Wound Healing, ACS Nano 12 (2018) 1747-1759.
[32] C. Prasad, H. Tang, I. Bahadur, Graphitic carbon nitride based ternary nanocomposites: From synthesis to their applications in photocatalysis: A recent review, Journal of Molecular Liquids 281 (2019) 634-654.
[33] E. Kroke, M. Schwarz, E. Horath-Bordon, P. Kroll, B. Noll, A.D. Norman, Tri-s-triazine derivatives. Part I. From trichloro-tri-s-triazine to graphitic C 3 N 4 structures, New Journal of Chemistry 26 (2002) 508-512.
[34] P. Murugesan, J.A. Moses, C. Anandharamakrishnan, Photocatalytic disinfection efficiency of 2D structure graphitic carbon nitride-based nanocomposites: a review, Journal of Materials Science 54 (2019) 12206-12235.
[35] C. Zhang, W. Wang, A. Duan, G. Zeng, D. Huang, C. Lai, X. Tan, M. Cheng, R. Wang, C. Zhou, W. Xiong, Y. Yang, Adsorption behavior of engineered carbons and carbon nanomaterials for metal endocrine disruptors: Experiments and theoretical calculation, Chemosphere 222 (2019) 184-194.
[36] W. Wang, M. Chen, D. Huang, G. Zeng, C. Zhang, C. Lai, C. Zhou, Y. Yang, M. Cheng, L. Hu, W. Xiong, Z. Li, Z. Wang, An overview on nitride and nitrogen-doped photocatalysts for energy and environmental applications, Composites Part B: Engineering 172 (2019) 704-723.
[37] J. Yang, X. Liu, X. Liu, Q. Xu, W. Wang, D. Wang, G. Yang, Q. Fu, Z. Kang, Q. Yang, Y. Liu, Q. Wang, B.-J. Ni, Enhanced dark fermentative hydrogen production from waste activated sludge by combining potassium ferrate with alkaline pretreatment, Science of The Total Environment 707 (2020) 136105.
[38] Z. Wang, H. Wang, Z. Zeng, G. Zeng, P. Xu, R. Xiao, D. Huang, X. Chen, L. He, C. Zhou, Metal-organic frameworks derived Bi2O2CO3/porous carbon nitride: A nanosized Z-scheme systems with enhanced photocatalytic activity, Applied Catalysis B: Environmental 267 (2020) 118700.
[39] J.N. Tiwari, R.N. Tiwari, K.S. Kim, Zero-dimensional, one-dimensional, two-dimensional and three-dimensional nanostructured materials for advanced electrochemical energy devices, Progress in Materials Science 57 (2012) 724-803.
[40] F. Lu, W. Cai, Y. Zhang, ZnO Hierarchical Micro/Nanoarchitectures: Solvothermal Synthesis and Structurally Enhanced Photocatalytic Performance, Advanced Functional Materials 18 (2008) 1047-1056.

[41] J. Xu, Z. Wang, Y. Zhu, Enhanced Visible-Light-Driven Photocatalytic Disinfection Performance and Organic Pollutant Degradation Activity of Porous g-C3N4 Nanosheets, ACS applied materials & interfaces 9 (2017) 27727-27735.
[42] J. Huang, W. Ho, X. Wang, Metal-free disinfection effects induced by graphitic carbon nitride polymers under visible light illumination, Chemical communications 50 (2014) 4338-4340.
[43] S. Kang, W. Huang, L. Zhang, M. He, S. Xu, D. Sun, X. Jiang, Moderate Bacterial Etching Allows Scalable and Clean Delamination of g-C3N4 with Enriched Unpaired Electrons for Highly Improved Photocatalytic Water Disinfection, ACS applied materials & interfaces 10 (2018) 13796-13804.
[44] E.-j. Kan, Z. Li, J. Yang, J. Hou, Half-metallicity in edge-modified zigzag graphene nanoribbons, Journal of the American Chemical Society 130 (2008) 4224-4225.
[45] X. Wang, X. Li, L. Zhang, Y. Yoon, P.K. Weber, H. Wang, J. Guo, H. Dai, N-doping of graphene through electrothermal reactions with ammonia, Science 324 (2009) 768-771.
[46] Z. Teng, N. Yang, H. Lv, S. Wang, M. Hu, C. Wang, D. Wang, G. Wang, Edge-Functionalized g-C3N4 Nanosheets as a Highly Efficient Metal-free Photocatalyst for Safe Drinking Water, Chem 5 (2019) 664-680.
[47] H. Zhao, H. Yu, X. Quan, S. Chen, Y. Zhang, H. Zhao, H. Wang, Fabrication of atomic single layer graphitic-C3N4 and its high performance of photocatalytic disinfection under visible light irradiation, Applied Catalysis B: Environmental 152-153 (2014) 46-50.
[48] X. Zhang, X. Xie, H. Wang, J. Zhang, B. Pan, Y. Xie, Enhanced Photoresponsive Ultrathin Graphitic-Phase C3N4 Nanosheets for Bioimaging, Journal of the American Chemical Society 135 (2013) 18-21.
[49] J. Xu, L. Zhang, R. Shi, Y. Zhu, Chemical exfoliation of graphitic carbon nitride for efficient heterogeneous photocatalysis, Journal of Materials Chemistry A 1 (2013) 14766.
[50] D. He, C. Zhang, G. Zeng, Y. Yang, D. Huang, L. Wang, H. Wang, A multifunctional platform by controlling of carbon nitride in the core-shell structure: From design to construction, and catalysis applications, Applied Catalysis B: Environmental 258 (2019) 117957.
[51] R. Ghosh Chaudhuri, S. Paria, Core/shell nanoparticles: classes, properties, synthesis mechanisms, characterization, and applications, Chemical reviews 112 (2011) 2373-2433.
[52] X. Yue, S. Yi, R. Wang, Z. Zhang, S. Qiu, Well-controlled SrTiO3@Mo2C core-shell nanofiber photocatalyst: Boosted photo-generated charge carriers transportation and enhanced catalytic performance for water reduction, Nano Energy 47 (2018) 463-473.
[53] C. Feng, Y. Deng, L. Tang, G. Zeng, J. Wang, J. Yu, Y. Liu, B. Peng, H. Feng, J. Wang, Core-shell Ag2CrO4/N-GQDs@g-C3N4 composites with anti-photocorrosion performance for enhanced full-spectrum-light photocatalytic activities, Applied Catalysis B: Environmental 239 (2018) 525-536.
[54] J. Song, X. Wu, M. Zhang, C. Liu, J. Yu, G. Sun, Y. Si, B. Ding, Highly flexible, core-shell heterostructured, and visible-light-driven titania-based nanofibrous membranes for antibiotic removal and E. coil inactivation, Chemical Engineering Journal 379 (2020) 122269.
[55] S. Wang, C. Li, T. Wang, P. Zhang, A. Li, J. Gong, Controllable synthesis of nanotube-type graphitic C 3 N 4 and their visible-light photocatalytic and fluorescent properties, Journal of Materials Chemistry A 2 (2014) 2885-2890.
[56] H.W. Liang, S. Liu, S.H. Yu, Controlled synthesis of one‐dimensional inorganic nanostructures using pre‐existing one‐dimensional nanostructures as templates, Advanced materials 22 (2010) 3925-3937.
[57] W. Wang, Z. Zeng, G. Zeng, C. Zhang, R. Xiao, C. Zhou, W. Xiong, Y. Yang, L. Lei, Y. Liu, D. Huang, M.

Cheng, Y. Yang, Y. Fu, H. Luo, Y. Zhou, Sulfur doped carbon quantum dots loaded hollow tubular g-C3N4 as novel photocatalyst for destruction of Escherichia coli and tetracycline degradation under visible light, Chemical Engineering Journal 378 (2019) 122132.
[58] L. Jiang, X. Yuan, Y. Pan, J. Liang, G. Zeng, Z. Wu, H. Wang, Doping of graphitic carbon nitride for photocatalysis: A reveiw, Applied Catalysis B: Environmental 217 (2017) 388-406.
[59] W. Wang, P. Xu, M. Chen, G. Zeng, C. Zhang, C. Zhou, Y. Yang, D. Huang, C. Lai, M. Cheng, L. Hu, W. Xiong, H. Guo, M. Zhou, Alkali Metal-Assisted Synthesis of Graphite Carbon Nitride with Tunable Band-Gap for Enhanced Visible-Light-Driven Photocatalytic Performance, ACS Sustainable Chemistry & Engineering 6 (2018) 15503-15516.
[60] P. Zhang, X. Tan, S. Liu, Y. Liu, G. Zeng, S. Ye, Z. Yin, X. Hu, N. Liu, Catalytic degradation of estrogen by persulfate activated with iron-doped graphitic biochar: Process variables effects and matrix effects, Chemical Engineering Journal 378 (2019) 122141.
[61] M. Jia, Z. Yang, H. Xu, P. Song, W. Xiong, J. Cao, Y. Zhang, Y. Xiang, J. Hu, C. Zhou, Integrating N and F co-doped TiO2 nanotubes with ZIF-8 as photoelectrode for enhanced photo-electrocatalytic degradation of sulfamethazine, Chemical Engineering Journal 388 (2020) 124388.
[62] Y. Fu, G. Zeng, C. Lai, D. Huang, L. Qin, H. Yi, X. Liu, M. Zhang, B. Li, S. Liu, Hybrid architectures based on noble metals and carbon-based dots nanomaterials: A review of recent progress in synthesis and applications, Chemical Engineering Journal (2020) 125743.
[63] W. Wang, G. Li, T. An, D.K. Chan, C.Y. Jimmy, P.K. Wong, Photocatalytic hydrogen evolution and bacterial inactivation utilizing sonochemical-synthesized g-C3N4/red phosphorus hybrid nanosheets as a wide-spectral-responsive photocatalyst: the role of type I band alignment, Applied Catalysis B: Environmental 238 (2018) 126-135.
[64] C. Zhang, M. Zhang, Y. Li, D. Shuai, Visible-light-driven photocatalytic disinfection of human adenovirus by a novel heterostructure of oxygen-doped graphitic carbon nitride and hydrothermal carbonation carbon, Applied Catalysis B: Environmental 248 (2019) 11-21.
[65] Y. Zeng, X. Liu, C. Liu, L. Wang, Y. Xia, S. Zhang, S. Luo, Y. Pei, Scalable one-step production of porous oxygen-doped g-C3N4 nanorods with effective electron separation for excellent visible-light photocatalytic activity, Applied Catalysis B: Environmental 224 (2018) 1-9.
[66] D. Chen, J. Liu, Z. Jia, J. Fang, F. Yang, Y. Tang, K. Wu, Z. Liu, Z. Fang, Efficient visible-light-driven hydrogen evolution and Cr (VI) reduction over porous P and Mo co-doped g-C3N4 with feeble N vacancies photocatalyst, Journal of hazardous materials 361 (2019) 294-304.
[67] Q. Liu, J. Shen, X. Yu, X. Yang, W. Liu, J. Yang, H. Tang, H. Xu, H. Li, Y. Li, J. Xu, Unveiling the origin of boosted photocatalytic hydrogen evolution in simultaneously (S, P, O)-Codoped and exfoliated ultrathin g-C3N4 nanosheets, Applied Catalysis B: Environmental 248 (2019) 84-94.
[68] X. Xu, S. Wang, X. Yu, J. Dawa, D. Gui, R. Tang, Biosynthesis of Ag deposited phosphorus and sulfur co-doped g-C3N4 with enhanced photocatalytic inactivation performance under visible light, Applied Surface Science 501 (2020) 144245.
[69] P. Niu, M. Qiao, Y. Li, L. Huang, T. Zhai, Distinctive defects engineering in graphitic carbon nitride for greatly extended visible light photocatalytic hydrogen evolution, Nano Energy 44 (2018) 73-81.
[70] L. Shi, L. Yang, W. Zhou, Y. Liu, L. Yin, X. Hai, H. Song, J. Ye, Photoassisted Construction of Holey Defective g‐C3N4 Photocatalysts for Efficient Visible‐Light‐Driven H2O2 Production, Small 14 (2018) 1703142.
[71] Y. Jiang, Z. Sun, C. Tang, Y. Zhou, L. Zeng, L. Huang, Enhancement of photocatalytic hydrogen evolution activity of porous oxygen doped g-C3N4 with nitrogen defects induced by changing electron

transition, Applied Catalysis B: Environmental 240 (2019) 30-38.
[72] H. Yu, R. Shi, Y. Zhao, T. Bian, Y. Zhao, C. Zhou, G.I. Waterhouse, L.Z. Wu, C.H. Tung, T. Zhang, Alkali‐assisted synthesis of nitrogen deficient graphitic carbon nitride with tunable band Structures for efficient visible‐light‐driven hydrogen evolution, Advanced materials 29 (2017) 1605148.
[73] P. Niu, L.C. Yin, Y.Q. Yang, G. Liu, H.M. Cheng, Increasing the visible light absorption of graphitic carbon nitride (Melon) photocatalysts by homogeneous self‐modification with nitrogen vacancies, Advanced materials 26 (2014) 8046-8052.
[74] Y. Kang, Y. Yang, L.C. Yin, X. Kang, L. Wang, G. Liu, H.M. Cheng, Selective breaking of hydrogen bonds of layered carbon nitride for visible light photocatalysis, Advanced materials 28 (2016) 6471-6477.
[75] H. Liu, S. Ma, L. Shao, H. Liu, Q. Gao, B. Li, H. Fu, S. Fu, H. Ye, F. Zhao, J. Zhou, Defective engineering in graphitic carbon nitride nanosheet for efficient photocatalytic pathogenic bacteria disinfection, Applied Catalysis B: Environmental 261 (2020) 118201.
[76] Z. Zhao, Y. Sun, F. Dong, Graphitic carbon nitride based nanocomposites: a review, Nanoscale 7 (2015) 15-37.
[77] S. Mubeen, J. Lee, N. Singh, S. Krämer, G.D. Stucky, M. Moskovits, An autonomous photosynthetic device in which all charge carriers derive from surface plasmons, Nature nanotechnology 8 (2013) 247.
[78] S.N. Basahel, K. Lee, R. Hahn, P. Schmuki, S.M. Bawaked, S.A. Al-Thabaiti, Self-decoration of Pt metal particles on TiO2 nanotubes used for highly efficient photocatalytic H2 production, Chemical communications 50 (2014) 6123-6125.
[79] Y. Zheng, Z. Yu, H. Ou, A.M. Asiri, Y. Chen, X. Wang, Black Phosphorus and Polymeric Carbon Nitride Heterostructure for Photoinduced Molecular Oxygen Activation, Advanced Functional Materials 28 (2018) 1705407.
[80] Y. Yang, C. Zhang, D. Huang, G. Zeng, J. Huang, C. Lai, C. Zhou, W. Wang, H. Guo, W. Xue, R. Deng, M. Cheng, W. Xiong, Boron nitride quantum dots decorated ultrathin porous g-C3N4: Intensified exciton dissociation and charge transfer for promoting visible-light-driven molecular oxygen activation, Applied Catalysis B: Environmental 245 (2019) 87-99.
[81] Y. Fu, P. Xu, D. Huang, G. Zeng, C. Lai, L. Qin, B. Li, J. He, H. Yi, M. Cheng, C. Zhang, Au nanoparticles decorated on activated coke via a facile preparation for efficient catalytic reduction of nitrophenols and azo dyes, Applied Surface Science 473 (2019) 578-588.
[82] S. Ma, S. Zhan, Y. Jia, Q. Shi, Q. Zhou, Enhanced disinfection application of Ag-modified g-C3N4 composite under visible light, Applied Catalysis B: Environmental 186 (2016) 77-87.
[83] Y. Liu, X. Zeng, X. Hu, J. Hu, X. Zhang, Two-dimensional nanomaterials for photocatalytic water disinfection: recent progress and future challenges, Journal of Chemical Technology & Biotechnology 94 (2019) 22-37.
[84] J. Xu, Q. Gao, X. Bai, Z. Wang, Y. Zhu, Enhanced visible-light-induced photocatalytic degradation and disinfection activities of oxidized porous g-C3N4 by loading Ag nanoparticles, Catalysis Today 332 (2019) 227-235.
[85] Z. Wang, K. Dong, Z. Liu, Y. Zhang, Z. Chen, H. Sun, J. Ren, X. Qu, Activation of biologically relevant levels of reactive oxygen species by Au/g-C3N4 hybrid nanozyme for bacteria killing and wound disinfection, Biomaterials 113 (2017) 145-157.
[86] Q. Wang, X. Wang, Z. Yu, X. Jiang, J. Chen, L. Tao, M. Wang, Y. Shen, Artificial photosynthesis of ethanol using type-II g-C3N4/ZnTe heterojunction in photoelectrochemical CO2 reduction system, Nano Energy 60 (2019) 827-835.

[87] D. Huang, S. Chen, G. Zeng, X. Gong, C. Zhou, M. Cheng, W. Xue, X. Yan, J. Li, Artificial Z-scheme photocatalytic system: What have been done and where to go?, Coordination Chemistry Reviews 385 (2019) 44-80.
[88] Y. Liu, M. Cheng, Z. Liu, G. Zeng, H. Zhong, M. Chen, C. Zhou, W. Xiong, B. Shao, B. Song, Heterogeneous Fenton-like catalyst for treatment of rhamnolipid-solubilized hexadecane wastewater, Chemosphere 236 (2019) 124387.
[89] S.j. Liu, Y.g. Liu, X.f. Tan, S.b. Liu, M.f. Li, N. Liu, Z.h. Yin, S.r. Tian, Y.h. Zhou, Facile synthesis of MnOx‐loaded biochar for the removal of doxycycline hydrochloride: Effects of ambient conditions and co‐existing heavy metals, Journal of Chemical Technology & Biotechnology 94 (2019) 2187-2197.
[90] S. Chen, D. Huang, G. Zeng, X. Gong, W. Xue, J. Li, Y. Yang, C. Zhou, Z. Li, X. Yan, Modifying delafossite silver ferrite with polyaniline: Visible-light-response Z-scheme heterojunction with charge transfer driven by internal electric field, Chemical Engineering Journal 370 (2019) 1087-1100.
[91] W. Wang, J.C. Yu, D. Xia, P.K. Wong, Y. Li, Graphene and g-C3N4 nanosheets cowrapped elemental alpha-sulfur as a novel metal-free heterojunction photocatalyst for bacterial inactivation under visible-light, Environ Sci Technol 47 (2013) 8724-8732.
[92] F. Li, X. Jiang, J. Zhao, S. Zhang, Graphene oxide: A promising nanomaterial for energy and environmental applications, Nano energy 16 (2015) 488-515.
[93] X. Zou, L. Zhang, Z. Wang, Y. Luo, Mechanisms of the antimicrobial activities of graphene materials, Journal of the American Chemical Society 138 (2016) 2064-2077.
[94] L. Sun, T. Du, C. Hu, J. Chen, J. Lu, Z. Lu, H. Han, Antibacterial Activity of Graphene Oxide/g-C3N4 Composite through Photocatalytic Disinfection under Visible Light, ACS Sustainable Chemistry & Engineering 5 (2017) 8693-8701.
[95] K. Ouyang, K. Dai, H. Chen, Q. Huang, C. Gao, P. Cai, Metal-free inactivation of E. coli O157: H7 by fullerene/C3N4 hybrid under visible light irradiation, Ecotoxicology and environmental safety 136 (2017) 40-45.
[96] R. Wang, X. Kong, W. Zhang, W. Zhu, L. Huang, J. Wang, X. Zhang, X. Liu, N. Hu, Y. Suo, J. Wang, Mechanism insight into rapid photocatalytic disinfection of Salmonella based on vanadate QDs-interspersed g-C3N4 heterostructures, Applied Catalysis B: Environmental 225 (2018) 228-237.
[97] J.A. Caputo, L.C. Frenette, N. Zhao, K.L. Sowers, T.D. Krauss, D.J. Weix, General and efficient C–C bond forming photoredox catalysis with semiconductor quantum dots, Journal of the American Chemical Society 139 (2017) 4250-4253.
[98] S.Y. Lim, W. Shen, Z. Gao, Carbon quantum dots and their applications, Chemical Society reviews 44 (2015) 362-381.
[99] A. Boulesbaa, K. Wang, M. Mahjouri-Samani, M. Tian, A.A. Puretzky, I. Ivanov, C.M. Rouleau, K. Xiao, B.G. Sumpter, D.B. Geohegan, Ultrafast Charge Transfer and Hybrid Exciton Formation in 2D/0D Heterostructures, Journal of the American Chemical Society 138 (2016) 14713-14719.
[100] Q. Zhang, X. Quan, H. Wang, S. Chen, Y. Su, Z. Li, Constructing a visible-light-driven photocatalytic membrane by gC 3 N 4 quantum dots and TiO 2 nanotube array for enhanced water treatment, Scientific reports 7 (2017) 3128.
[101] Y.-Y. Yang, X.-G. Zhang, C.-G. Niu, H.-P. Feng, P.-Z. Qin, H. Guo, C. Liang, L. Zhang, H.-Y. Liu, L. Li, Dual-channel charges transfer strategy with synergistic effect of Z-scheme heterojunction and LSPR effect for enhanced quasi-full-spectrum photocatalytic bacterial inactivation: new insight into interfacial charge transfer and molecular oxygen activation, Applied Catalysis B: Environmental 264 (2020) 118465.

[102] G. Li, X. Nie, J. Chen, Q. Jiang, T. An, P.K. Wong, H. Zhang, H. Zhao, H. Yamashita, Enhanced visible-light-driven photocatalytic inactivation of Escherichia coli using g-C3N4/TiO2 hybrid photocatalyst synthesized using a hydrothermal-calcination approach, Water research 86 (2015) 17-24.
[103] B. Wu, Y. Li, K. Su, L. Tan, X. Liu, Z. Cui, X. Yang, Y. Liang, Z. Li, S. Zhu, K.W.K. Yeung, S. Wu, The enhanced photocatalytic properties of MnO2/g-C3N4 heterostructure for rapid sterilization under visible light, Journal of hazardous materials 377 (2019) 227-236.
[104] J. Xu, Y. Li, X. Zhou, Y. Li, Z.D. Gao, Y.Y. Song, P. Schmuki, Graphitic C3N4 - Sensitized TiO2 Nanotube Layers: A Visible - Light Activated Efficient Metal - Free Antimicrobial Platform, Chemistry – A European Journal 22 (2016) 3947-3951.
[105] I.M. Sundaram, S. Kalimuthu, G. Ponniah, Highly active ZnO modified g-C3N4 Nanocomposite for dye degradation under UV and Visible Light with enhanced stability and antimicrobial activity, Composites Communications 5 (2017) 64-71.
[106] Z. Jiang, B. Wang, Y. Li, H.S. Chan, H. Sun, T. Wang, H. Li, S. Yuan, M.K.H. Leung, A. Lu, P.K. Wong, Solar-light-driven rapid water disinfection by ultrathin magnesium titanate/carbon nitride hybrid photocatalyst: Band structure analysis and role of reactive oxygen species, Applied Catalysis B: Environmental 257 (2019) 117898.
[107] Y. Li, Y. Li, S. Ma, P. Wang, Q. Hou, J. Han, S. Zhan, Efficient water disinfection with Ag2WO4-doped mesoporous g-C3N4 under visible light, Journal of hazardous materials 338 (2017) 33-46.
[108] Y.Y. Yang, C.G. Niu, X.J. Wen, L. Zhang, C. Liang, H. Guo, D.L. Guan, H.Y. Liu, G.M. Zeng, Fabrication of visible-light-driven silver iodide modified iodine-deficient bismuth oxyiodides Z-scheme heterojunctions with enhanced photocatalytic activity for Escherichia coli inactivation and tetracycline degradation, Journal of colloid and interface science 533 (2019) 636-648.
[109] L. Wang, Z. Yuan, H.E. Karahan, Y. Wang, X. Sui, F. Liu, Y. Chen, Nanocarbon materials in water disinfection: state-of-the-art and future directions, Nanoscale 11 (2019) 9819-9839.
[110] J. You, Y. Guo, R. Guo, X. Liu, A review of visible light-active photocatalysts for water disinfection: Features and prospects, Chemical Engineering Journal 373 (2019) 624-641.
[111] C. Zhang, Y. Li, D. Shuai, W. Zhang, L. Niu, L. Wang, H. Zhang, Visible-light-driven, water-surface-floating antimicrobials developed from graphitic carbon nitride and expanded perlite for water disinfection, Chemosphere 208 (2018) 84-92.
[112] Z. Wang, M. Chen, D. Huang, G. Zeng, P. Xu, C. Zhou, C. Lai, H. Wang, M. Cheng, W. Wang, Multiply structural optimized strategies for bismuth oxyhalide photocatalysis and their environmental application, Chemical Engineering Journal 374 (2019) 1025-1045.
[113] H. Yu, L. Jiang, H. Wang, B. Huang, X. Yuan, J. Huang, J. Zhang, G. Zeng, Modulation of Bi2 MoO6 -Based Materials for Photocatalytic Water Splitting and Environmental Application: a Critical Review, Small 15 (2019) e1901008.
[114] J. Liang, F. Liu, M. Li, W. Liu, M. Tong, Facile synthesis of magnetic Fe3O4@BiOI@AgI for water decontamination with visible light irradiation: Different mechanisms for different organic pollutants degradation and bacterial disinfection, Water research 137 (2018) 120-129.
[115] J. Liang, C. Shan, X. Zhang, M. Tong, Bactericidal mechanism of BiOI–AgI under visible light irradiation, Chemical Engineering Journal 279 (2015) 277-285.
[116] X. Zhang, L. Zhang, Electronic and band structure tuning of ternary semiconductor photocatalysts by self doping: the case of BiOI, The Journal of Physical Chemistry C 114 (2010)

18198-18206.
[117] Y. Zhang, M. Zhang, L. Tang, J. Wang, Y. Zhu, C. Feng, Y. Deng, W. He, Y. Hu, Platinum like cocatalysts tungsten carbide loaded hollow tubular g-C3N4 achieving effective space separation of carriers to degrade antibiotics, Chemical Engineering Journal (2019) 123487.
[118] J. Li, Y. Yin, E. Liu, Y. Ma, J. Wan, J. Fan, X. Hu, In situ growing Bi2MoO6 on g-C3N4 nanosheets with enhanced photocatalytic hydrogen evolution and disinfection of bacteria under visible light irradiation, Journal of hazardous materials 321 (2017) 183-192.
[119] Y. Yang, C. Zhang, C. Lai, G. Zeng, D. Huang, M. Cheng, J. Wang, F. Chen, C. Zhou, W. Xiong, BiOX (X= Cl, Br, I) photocatalytic nanomaterials: applications for fuels and environmental management, Advances in colloid and interface science 254 (2018) 76-93.
[120] X. Liu, Z. Ni, Y. He, N. Su, R. Guo, Q. Wang, T. Yi, Ultrasound-assisted two-step water-bath synthesis of g-C3N4/BiOBr composites: visible light-driven photocatalysis, sterilization, and reaction mechanism, New Journal of Chemistry 43 (2019) 8711-8721.
[121] D. Xia, W. Wang, R. Yin, Z. Jiang, T. An, G. Li, H. Zhao, P.K. Wong, Enhanced photocatalytic inactivation of Escherichia coli by a novel Z-scheme g-C 3 N 4 /m-Bi 2 O 4 hybrid photocatalyst under visible light: The role of reactive oxygen species, Applied Catalysis B: Environmental 214 (2017) 23-33.
[122] B. Pant, M. Park, J.H. Lee, H.-Y. Kim, S.-J. Park, Novel magnetically separable silver-iron oxide nanoparticles decorated graphitic carbon nitride nano-sheets: A multifunctional photocatalyst via one-step hydrothermal process, Journal of colloid and interface science 496 (2017) 343-352.
[123] M. Zhang, C. Lai, B. Li, D. Huang, G. Zeng, P. Xu, L. Qin, S. Liu, X. Liu, H. Yi, Rational design 2D/2D BiOBr/CDs/g-C3N4 Z-scheme heterojunction photocatalyst with carbon dots as solid-state electron mediators for enhanced visible and NIR photocatalytic activity: Kinetics, intermediates, and mechanism insight, Journal of catalysis 369 (2019) 469-481.
[124] D. Vidyasagar, S.G. Ghugal, A. Kulkarni, P. Mishra, A.G. Shende, S.S. Umare, R. Sasikala, Silver/Silver (II) oxide (Ag/AgO) loaded graphitic carbon nitride microspheres: An effective visible light active photocatalyst for degradation of acidic dyes and bacterial inactivation, Applied catalysis B: environmental 221 (2018) 339-348.
[125] F. Chen, Q. Yang, Y. Wang, J. Zhao, D. Wang, X. Li, Z. Guo, H. Wang, Y. Deng, C. Niu, Novel ternary heterojunction photcocatalyst of Ag nanoparticles and g-C3N4 nanosheets co-modified BiVO4 for wider spectrum visible-light photocatalytic degradation of refractory pollutant, Applied Catalysis B: Environmental 205 (2017) 133-147.
[126] X. Zeng, S. Lan, I.M. Lo, Rapid disinfection of E. coli by a ternary BiVO 4/Ag/gC 3 N 4 composite under visible light: photocatalytic mechanism and performance investigation in authentic sewage, Environmental Science: Nano 6 (2019) 610-623.
[127] K. Shen, M.A. Gondal, R.G. Siddique, S. Shi, S. Wang, J. Sun, Q. Xu, Preparation of ternary Ag/Ag3PO4/g-C3N4 hybrid photocatalysts and their enhanced photocatalytic activity driven by visible light, Chinese Journal of Catalysis 35 (2014) 78-84.
[128] Y. Tian, F. Zhou, S. Zhan, Z. Zhu, Q. He, Mechanisms on the enhanced sterilization performance of fluorocarbon resin composite coatings modified by g-C3N4/Bi2MoO6 under the visible-light, Journal of Photochemistry and Photobiology A: Chemistry 350 (2018) 10-16.
[129] M. Faraji, N. Mohaghegh, A. Abedini, Ternary composite of TiO2 nanotubes/Ti plates modified by g-C3N4 and SnO2 with enhanced photocatalytic activity for enhancing antibacterial and photocatalytic activity, Journal of Photochemistry and Photobiology B: Biology 178 (2018) 124-132.
[130] J. Song, X. Wang, J. Ma, X. Wang, J. Wang, S. Xia, J. Zhao, Removal of Microcystis aeruginosa and

Microcystin-LR using a graphitic-C3N4/TiO2 floating photocatalyst under visible light irradiation, Chemical Engineering Journal 348 (2018) 380-388.
[131] Y. Hou, Z. Wen, S. Cui, X. Guo, J. Chen, Constructing 2D porous graphitic C3N4 nanosheets/nitrogen‐doped graphene/layered MoS2 ternary nanojunction with enhanced photoelectrochemical activity, Advanced materials 25 (2013) 6291-6297.
[132] B. Liu, X. Han, Y. Wang, X. Fan, Z. Wang, J. Zhang, H. Shi, Synthesis of gC 3 N 4/BiOI/BiOBr heterostructures for efficient visible-light-induced photocatalytic and antibacterial activity, Journal of Materials Science: Materials in Electronics 29 (2018) 14300-14310.
[133] C. Li, Z. Sun, W. Zhang, C. Yu, S. Zheng, Highly efficient g-C3N4/TiO2/kaolinite composite with novel three-dimensional structure and enhanced visible light responding ability towards ciprofloxacin and S. aureus, Applied Catalysis B: Environmental 220 (2018) 272-282.
[134] A. Markowska-Szczupak, K. Ulfig, A. Morawski, The application of titanium dioxide for deactivation of bioparticulates: an overview, Catalysis Today 169 (2011) 249-257.
[135] J. Bogdan, J. Zarzyńska, J. Pławińska-Czarnak, Comparison of infectious agents susceptibility to photocatalytic effects of nanosized titanium and zinc oxides: a practical approach, Nanoscale research letters 10 (2015) 309.
[136] H. Ishiguro, R. Nakano, Y. Yao, J. Kajioka, A. Fujishima, K. Sunada, M. Minoshima, K. Hashimoto, Y. Kubota, Photocatalytic inactivation of bacteriophages by TiO 2-coated glass plates under low-intensity, long-wavelength UV irradiation, Photochemical & Photobiological Sciences 10 (2011) 1825-1829.
[137] P. Liu, W. Duan, Q. Wang, X. Li, The damage of outer membrane of Escherichia coli in the presence of TiO 2 combined with UV light, Colloids and Surfaces B: Biointerfaces 78 (2010) 171-176.
[138] G. Liu, S. Zhang, K. Yang, L. Zhu, D. Lin, Toxicity of perfluorooctane sulfonate and perfluorooctanoic acid to Escherichia coli: Membrane disruption, oxidative stress, and DNA damage induced cell inactivation and/or death, Environmental Pollution 214 (2016) 806-815.
[139] X. Zheng, Z.-p. Shen, C. Cheng, L. Shi, R. Cheng, D.-h. Yuan, Photocatalytic disinfection performance in virus and virus/bacteria system by Cu-TiO2 nanofibers under visible light, Environmental pollution 237 (2018) 452-459.
[140] A. Benabbou, Z. Derriche, C. Felix, P. Lejeune, C. Guillard, Photocatalytic inactivation of Escherischia coli: Effect of concentration of TiO2 and microorganism, nature, and intensity of UV irradiation, Applied Catalysis B: Environmental 76 (2007) 257-263.
[141] Y. Li, C. Zhang, D. Shuai, S. Naraginti, D. Wang, W. Zhang, Visible-light-driven photocatalytic inactivation of MS2 by metal-free g-C3N4: Virucidal performance and mechanism, Water research 106 (2016) 249-258.
[142] C. Zhang, Y. Li, D. Shuai, Y. Shen, D. Wang, Progress and challenges in photocatalytic disinfection of waterborne Viruses: A review to fill current knowledge gaps, Chemical Engineering Journal 355 (2019) 399-415.
[143] S. Feng, T. Chen, Z. Liu, J. Shi, X. Yue, Y. Li, Z-scheme CdS/CQDs/g-C3N4 composites with visible-near-infrared light response for efficient photocatalytic organic pollutant degradation, Science of The Total Environment (2019) 135404.
[144] H. Che, G. Che, P. Zhou, C. Liu, H. Dong, C. Li, N. Song, C. Li, Nitrogen doped carbon ribbons modified g-C3N4 for markedly enhanced photocatalytic H2-production in visible to near-infrared region, Chemical Engineering Journal 382 (2020) 122870.
[145] A.G. Rincón, C. Pulgarin, Photocatalytical inactivation of E. coli: effect of (continuous–intermittent) light intensity and of (suspended–fixed) TiO2 concentration, Applied Catalysis B:

Environmental 44 (2003) 263-284.
[146] J.E. Lee, G. Ko, Norovirus and MS2 inactivation kinetics of UV-A and UV-B with and without TiO2, Water research 47 (2013) 5607-5613.
[147] M.N. Chong, B. Jin, C.W. Chow, C. Saint, Recent developments in photocatalytic water treatment technology: a review, Water research 44 (2010) 2997-3027.
[148] T.W. Ng, L. Zhang, J. Liu, G. Huang, W. Wang, P.K. Wong, Visible-light-driven photocatalytic inactivation of Escherichia coli by magnetic Fe2O3–AgBr, Water research 90 (2016) 111-118.
[149] L. Lei, D. Huang, C. Zhang, R. Deng, S. Chen, Z. Li, F dopants triggered active sites in bifunctional cobalt sulfide@ nickel foam toward electrocatalytic overall water splitting in neutral and alkaline media: Experiments and theoretical calculations, Journal of Catalysis 385 (2020) 129-139.
[150] T. Tong, C.T.T. Binh, J.J. Kelly, J.-F. Gaillard, K.A. Gray, Cytotoxicity of commercial nano-TiO2 to Escherichia coli assessed by high-throughput screening: Effects of environmental factors, Water research 47 (2013) 2352-2362.
[151] B. Guo, S.D. Snow, B.J. Starr, I. Xagoraraki, V.V. Tarabara, Photocatalytic inactivation of human adenovirus 40: Effect of dissolved organic matter and prefiltration, Separation and Purification Technology 193 (2018) 193-201.
[152] M. Cheng, Y. Liu, D. Huang, C. Lai, G. Zeng, J. Huang, Z. Liu, C. Zhang, C. Zhou, L. Qin, Prussian blue analogue derived magnetic Cu-Fe oxide as a recyclable photo-Fenton catalyst for the efficient removal of sulfamethazine at near neutral pH values, Chemical Engineering Journal 362 (2019) 865-876.
[153] J. Wang, L. Tang, G. Zeng, Y. Deng, Y. Liu, L. Wang, Y. Zhou, Z. Guo, J. Wang, C. Zhang, Atomic scale g-C3N4/Bi2WO6 2D/2D heterojunction with enhanced photocatalytic degradation of ibuprofen under visible light irradiation, Applied Catalysis B: Environmental 209 (2017) 285-294.
[154] Y. Koizumi, M. Taya, Photocatalytic inactivation rate of phage MS2 in titanium dioxide suspensions containing various ionic species, Biotechnology Letters 24 (2002) 459-462.
[155] W. Wang, G. Huang, J.C. Yu, P.K. Wong, Advances in photocatalytic disinfection of bacteria: Development of photocatalysts and mechanisms, J Environ Sci (China) 34 (2015) 232-247.
[156] C. Zhang, Y. Li, D. Shuai, Y. Shen, W. Xiong, L. Wang, Graphitic carbon nitride (g-C3N4)-based photocatalysts for water disinfection and microbial control: A review, Chemosphere 214 (2019) 462-479.
[157] Y. Nosaka, A.Y. Nosaka, Generation and Detection of Reactive Oxygen Species in Photocatalysis, Chemical reviews 117 (2017) 11302-11336.
[158] M.E. Khan, T.H. Han, M.M. Khan, M.R. Karim, M.H. Cho, Environmentally sustainable fabrication of Ag@ g-C3N4 nanostructures and their multifunctional efficacy as antibacterial agents and photocatalysts, ACS Applied Nano Materials 1 (2018) 2912-2922.
[159] V. Shanmugam, A.L. Muppudathi, S. Jayavel, K.S. Jeyaperumal, Construction of high efficient g-C3N4 nanosheets combined with Bi2MoO6-Ag photocatalysts for visible-light-driven photocatalytic activity and inactivation of bacterias, Arabian Journal of Chemistry (2018).
[160] J.H. Thurston, N.M. Hunter, L.J. Wayment, K.A. Cornell, Urea-derived graphitic carbon nitride (ug-C3N4) films with highly enhanced antimicrobial and sporicidal activity, Journal of colloid and interface science 505 (2017) 910-918.
[161] T. Wang, Z. Jiang, T. An, G. Li, H. Zhao, P.K. Wong, Enhanced Visible-Light-Driven Photocatalytic Bacterial Inactivation by Ultrathin Carbon-Coated Magnetic Cobalt Ferrite Nanoparticles, Environ Sci Technol 52 (2018) 4774-4784.

[162] D. Wu, W. Wang, T.W. Ng, G. Huang, D. Xia, H.Y. Yip, H.K. Lee, G. Li, T. An, P.K. Wong, Visible-light-driven photocatalytic bacterial inactivation and the mechanism of zinc oxysulfide under LED light irradiation, Journal of Materials Chemistry A 4 (2016) 1052-1059.
[163] Y. Zhou, W. Wang, C. Zhang, D. Huang, C. Lai, M. Cheng, L. Qin, Y. Yang, C. Zhou, B. Li, H. Luo, D. He, Sustainable hydrogen production by molybdenum carbide-based efficient photocatalysts: From properties to mechanism, Advances in Colloid and Interface Science 279 (2020) 102144.
[164] Y. Yang, Z. Zeng, G. Zeng, D. Huang, R. Xiao, C. Zhang, C. Zhou, W. Xiong, W. Wang, M. Cheng, W. Xue, H. Guo, X. Tang, D. He, Ti3C2 Mxene/porous g-C3N4 interfacial Schottky junction for boosting spatial charge separation in photocatalytic H2O2 production, Applied Catalysis B: Environmental 258 (2019) 117956.
[165] C. Zhang, Y. Zhou, W. Wang, Y. Yang, C. Zhou, L. Wang, L. Lei, D. He, H. Luo, D. Huang, Formation of Mo2C/hollow tubular g-C3N4 hybrids with favorable charge transfer channels for excellent visible-light-photocatalytic performance, Applied Surface Science 527 (2020) 146757.
[166] Y. Yang, G. Zeng, D. Huang, C. Zhang, D. He, C. Zhou, W. Wang, W. Xiong, B. Song, H. Yi, S. Ye, X. Ren, In Situ Grown Single-Atom Cobalt on Polymeric Carbon Nitride with Bidentate Ligand for Efficient Photocatalytic Degradation of Refractory Antibiotics, Small n/a 2001634.
[167] M. Gao, T. An, G. Li, X. Nie, H.-Y. Yip, H. Zhao, P.-K. Wong, Genetic studies of the role of fatty acid and coenzyme A in photocatalytic inactivation of Escherichia coli, Water research 46 (2012) 3951-3957.
[168] T. Leung, C. Chan, C. Hu, J. Yu, P. Wong, Photocatalytic disinfection of marine bacteria using fluorescent light, Water research 42 (2008) 4827-4837.
[169] H. Sun, G. Li, T. An, H. Zhao, P.K. Wong, Unveiling the photoelectrocatalytic inactivation mechanism of Escherichia coli: Convincing evidence from responses of parent and anti-oxidation single gene knockout mutants, Water research 88 (2016) 135-143.
[170] T. An, H. Sun, G. Li, H. Zhao, P.K. Wong, Differences in photoelectrocatalytic inactivation processes between E. coli and its isogenic single gene knockoff mutants: Destruction of membrane framework or associated proteins?, Applied Catalysis B: Environmental 188 (2016) 360-366.
[171] J. Deng, J. Liang, M. Li, M. Tong, Enhanced visible-light-driven photocatalytic bacteria disinfection by g-C3N4-AgBr, Colloids and Surfaces B: Biointerfaces 152 (2017) 49-57.
[172] O. Akhavan, M. Choobtashani, E. Ghaderi, Protein degradation and RNA efflux of viruses photocatalyzed by graphene–tungsten oxide composite under visible light irradiation, The Journal of Physical Chemistry C 116 (2012) 9653-9659.
[173] X. Hu, L. Mu, J. Wen, Q. Zhou, Covalently synthesized graphene oxide-aptamer nanosheets for efficient visible-light photocatalysis of nucleic acids and proteins of viruses, Carbon 50 (2012) 2772-2781.
[174] M.V. Liga, E.L. Bryant, V.L. Colvin, Q. Li, Virus inactivation by silver doped titanium dioxide nanoparticles for drinking water treatment, Water research 45 (2011) 535-544.
[175] Y. Yamaguchi, S. Usuki, Y. Kanai, K. Yamatoya, N. Suzuki, K.-i. Katsumata, C. Terashima, T. Suzuki, A. Fujishima, H. Sakai, Selective inactivation of bacteriophage in the presence of bacteria by use of ground Rh-doped SrTiO3 photocatalyst and visible light, ACS applied materials & interfaces 9 (2017) 31393-31400.
[176] W. Wang, T. An, G. Li, D. Xia, H. Zhao, C.Y. Jimmy, P.K. Wong, Earth-abundant Ni2P/g-C3N4 lamellar nanohydrids for enhanced photocatalytic hydrogen evolution and bacterial inactivation under visible light irradiation, Applied Catalysis B: Environmental 217 (2017) 570-580.